POLITECNICO DI TORINO
Repository ISTITUZIONALE

Multiplicity dependence of +c and 0c production in pp collisions at s=13 TeV

Original
Multiplicity dependence of +c and 0c production in pp collisions at s=13 TeV / Null, N., Abualrob, I.J., Acharya, S., Aglieri Rinella, G., Aglietta, L., Agnello, M., Agrawal, N., Ahammed, Z., Ahmad, S., Ahuja, I., Akbar, Zul., Akindinov, A., Akishina, V., Al-Turany, M., Aleksandrov, D., Alessandro, B., Alfanda, H.M., Alfaro Molina, R., Ali, B., Alici, A., et al.. - In: JOURNAL OF HIGH ENERGY PHYSICS. - ISSN 1029-8479. - 2025:12(2025). [10.1007/jhep12(2025)038]

Availability:
This version is available at: 11583/3016103 since: 2026-09-29T20:38:27Z

Publisher:
Springer

Published
DOI:10.1007/jhep12(2025)038

Terms of use:

This article is made available under terms and conditions as specified in the corresponding bibliographic description in the repository

Publisher copyright

(Article begins on next page)

25 November 2026

Published for SISSA by Springer

Received: August 27, 2025
Revised: October 27, 2025
Accepted: October 28, 2025
Published: December 3, 2025

Multiplicity dependence of Ξ_c^+ and Ξ_c^0 production in pp collisions at $\sqrt{s} = 13$ TeV



The ALICE collaboration

E-mail: ALICE-publications@cern.ch

Abstract: The first measurement at midrapidity ($|y| < 0.5$) of the production yield of the strange-charm baryons Ξ_c^+ and Ξ_c^0 as a function of transverse momentum (p_T) in different charged-particle multiplicity classes in proton-proton collisions at $\sqrt{s} = 13$ TeV with the ALICE experiment at the LHC is reported. The Ξ_c^+ baryon is reconstructed via the $\Xi_c^+ \to \Xi^-\pi^+\pi^+$ decay channel in the range $4 < p_T < 12$ GeV/c, while the Ξ_c^0 baryon is reconstructed via both the $\Xi_c^0 \to \Xi^-\pi^+$ and $\Xi_c^0 \to \Xi^-e^+\nu_e$ decay channels in the range $2 < p_T < 12$ GeV/c. The baryon-to-meson ($\Xi_c^{0,+}/D^0$) and the baryon-to-baryon ($\Xi_c^{0,+}/\Lambda_c^+$) production yield ratios show no significant dependence on multiplicity. In addition, the observed yield ratios are not described by theoretical predictions that model charm-quark fragmentation based on measurements at e^+e^- and e^-p colliders, indicating differences in the charm-baryon production mechanism in pp collisions. A comparison with different event generators and tunings, including different modelling of the hadronisation process, is also discussed. Moreover, the branching-fraction ratio of $BR(\Xi_c^0 \to \Xi^-e^+\nu_e)/BR(\Xi_c^0 \to \Xi^-\pi^+)$ is measured as $0.825 \pm 0.094\,(stat.) \pm 0.081\,(syst.)$. This value supersedes the previous ALICE measurement, improving the statistical precision by a factor of 1.6.

Keywords: Charm Physics, Hadron-Hadron Scattering, Proton-Proton Scattering

ArXiv ePrint: 2508.09955

Open Access, Copyright CERN,
for the benefit of the ALICE Collaboration.
Article funded by SCOAP^3.

https://doi.org/10.1007/JHEP12(2025)038

JHEP12(2025)038

Contents

1 Introduction 1

2 Experimental apparatus and data sample 3

3 Data analysis 4

4 Systematic uncertainties 9

5 Results 12

6 Summary 16

A Systematic uncertainties for other multiplicity classes 18

The ALICE collaboration 24

1 Introduction

Heavy quarks, such as charm and beauty, are produced in hard-scattering processes occurring in the early stages of ultrarelativistic proton-proton (pp) collisions at the LHC. Therefore, measuring the production of hadrons containing at least one heavy quark provides a crucial test of perturbative Quantum Chromodynamics (pQCD) calculations. The production cross section of heavy-flavour hadrons, generally computed using a factorisation approach, is calculated as the convolution of three factors [1]: i) the Parton Distribution Functions (PDFs), which describe the probability distribution of finding quarks or gluons inside the incoming proton with a given fraction of the proton momentum; ii) the hard-scattering cross section at the partonic level, which governs the interaction between partons leading to the production of heavy quarks; and iii) the fragmentation functions, which model the transition of the heavy quark into a heavy-flavour hadron carrying a fraction of the quark momentum. The fragmentation functions cannot be computed using the pQCD approach. They are typically constrained by measurements in e^+e^- or e^-p collisions [2], assuming universal hadronisation. Measurements of heavy-flavour hadron production in pp collisions provide the essential ingredients for testing the universality of heavy-quark fragmentation functions, and ultimately the heavy-quark hadronisation process. The production yield ratios of different hadron species are an especially sensitive tool to investigate hadronisation mechanisms since the PDFs and partonic scattering cross sections are universal across all charm hadrons.

Extensive measurements of charm-hadron production including charm mesons: D^0, D^+, D_s^+, D^{*+}, $D_{s1}^+(2536)$, $D_{s2}^{*+}(2573)$ [3–10], and charm baryons: Λ_c^+, $\Sigma_c^{0,++}(2455)$, $\Xi_c^{0,+}$, Ω_c^0 [11–19], have been performed in pp collisions at the LHC [20]. The measurements of charm-meson production cross sections at midrapidity in pp collisions are well described over a wide range of transverse momentum (p_T) with respect to the beam axis, by perturbative calculations at next-to-leading order with next-to-leading-log resummation, such as the

JHEP12(2025)038

general-mass variable-flavour-number scheme (GM-VFNS [21–23]) and the fixed-order plus next-to-leading-log (FONLL [24, 25]) frameworks. Both calculations use fragmentation functions tuned on measurements in e^+e^- and e^-p collisions [2]. However, these models significantly underestimate charm-baryon production in pp collisions [3, 13]. Also, the measurements of the Λ_c^+/D^0 baryon-to-meson production yield ratio in pp collisions at $\sqrt{s}$ = 5.02, 7, and 13 TeV [3, 12, 16] show a strong p_T dependence, with a significant enhancement at $1 < p_T < 8$ GeV/c, compared to the results obtained in e^+e^- and e^-p collisions [2]. This enhancement also deviates from the predictions of event generators tuned to reproduce the results in e^+e^- collisions, such as PYTHIA 8 with the Monash tune [26]. A similar deviation between pp and e^+e^- collisions has been reported also for the beauty-quark baryon-to-meson production ratio, suggesting that the observed difference is not limited to the charm sector [27, 28]. These observations question the assumed universality of the charm-quark hadronisation process across different collision systems and suggest that the 'in-vacuum' string fragmentation alone fails to describe heavy-flavour baryon production in hadronic collisions. Recent ALICE measurements on charm fragmentation fractions in pp collisions at $\sqrt{s}$ = 5.02 and 13 TeV [11, 29] also support this conclusion.

The Λ_c^+/D^0 production ratio in pp collisions is well described by effective model calculations and event generators implementing different hadronisation mechanisms: i) a tune of the PYTHIA 8 event generator with colour reconnection beyond the leading-colour approximation (CR-BLC [30]), in which baryon production is enhanced by the introduction of new topologies for colour reconnection mechanisms as the junctions; ii) the Statistical Hadronisation Model (SHM) including higher-mass excited charm baryon states, which are predicted by the Relativistic Quark Model (RQM) [31] but have not yet been experimentally measured. The model replaces the complexity of the hadronisation process with thermo-statistical weights governed by the masses of available hadron states at a universal hadronisation temperature; and iii) models assuming a charm quark hadronisation via coalescence with other quarks produced in the collision, such as Catania [32, 33], Quark Combination Mode (QCM) [34], and POWLANG [35]. However, unlike the measurements of the Λ_c^+/D^0 and $\Sigma_c^{0,++}(2455)/D^0$ ratios [16] that are both described by such models within the measured uncertainties, the production ratios for strange-charm baryons, such as $\Xi_c^{0,+}/D^0$ and Ω_c^0/D^0, are not well described by these models [17, 19]. Studying charm-hadron production as a function of charged-particle multiplicity in pp collisions can extend the knowledge about how the charm-quark hadronisation mechanism evolves from low to high particle densities. Recent results of multiplicity-dependent Λ_c^+/D^0 production ratios in pp collisions [36] exhibit an increasing charm baryon-to-meson ratio with an increasing charged-particle multiplicity in the intermediate p_T region ($2 < p_T < 12$ GeV/c). However, at the same time, no significant multiplicity dependence is observed for the p_T-integrated yields within the current uncertainties. This weak multiplicity dependence of the p_T-integrated Λ_c^+/D^0 ratio is similar to that of Λ/K_S^0 [37]. Interestingly, a clear multiplicity dependence is observed in the multi-strange baryon-to-meson production yield ratios Ξ^-/K_S^0 and Ω^-/K_S^0. One possible explanation in the context of the Canonical Statistical Model (CSM) [38] is that moving from pp to Pb-Pb collisions the system volume increases, which gradually removes the canonical suppression associated with an exact charge conservation in pp collisions, leading to a global charge conservation in Pb-Pb collisions. Therefore, measurements of strange-charm baryon produc-

JHEP12(2025)038

Decay channel	BR (%)	Decay channel	BR (%)
$\Xi_c^+ \to \Xi^-\pi^+\pi^+$	2.86 ± 1.21 ± 0.38 [39]	$\Xi^- \to \Lambda\pi^-$	99.9 ± 0.04 [40]
$\Xi_c^0 \to \Xi^-\pi^+$	1.43 ± 0.27 [40]	$\Lambda \to p\pi^-$	64.1 ± 0.5 [40]
$\Xi_c^0 \to \Xi^-e^+\nu_e$	1.04 ± 0.24 [40]	-	-

Table 1. The branching ratios for the relevant decay channels.

tion in various multiplicity classes will offer key insights into hadron production mechanisms and their evolution with multiplicity density.

This article reports the p_T-differential production yields of prompt Ξ_c^+ and Ξ_c^0 baryons — produced either directly from a charm-quark hadronisation or from strong decays of excited charm-hadron states — measured in pp collisions at $\sqrt{s} = 13$ TeV at midrapidity ($|y| < 0.5$), in intervals of charged-particle multiplicity. The Ξ_c^+ baryon is reconstructed via the decay channel $\Xi_c^+ \to \Xi^-\pi^+\pi^+$ (and charge conjugates), in the interval $4 < p_T < 12$ GeV/c while the Ξ_c^0 baryon is reconstructed via the decay channels $\Xi_c^0 \to \Xi^-e^+\nu_e$ and $\Xi_c^0 \to \Xi^-\pi^+$ (and charge conjugates) in the interval $2 < p_T < 12$ GeV/c. The relevant branching ratios are summarised in table 1. The p_T-dependent $\Xi_c^{0,+}/\Lambda_c^+$ and $\Xi_c^{0,+}/D^0$ production yield ratios are also reported. In addition, the branching fraction ratio BR($\Xi_c^0 \to \Xi^-e^+\nu_e$)/BR($\Xi_c^0 \to \Xi^-\pi^+$) is measured with improved precision compared to previous results [17], thanks to the increased statistics.

This article is organised as follows: section 2 describes the experimental setup and the multiplicity determination, section 3 explains the analysis details, section 4 discusses the estimation of the systematic uncertainties, section 5 presents the results and comparisons to the model calculations, and section 6 concludes with a summary.

2 Experimental apparatus and data sample

Detailed descriptions of the ALICE apparatus and its LHC Run 2 performance are provided in refs. [41, 42]. In this section, the main detectors used for the analyses discussed in this article are briefly described. The central barrel detectors are located inside a cylindrical solenoid magnet, providing a magnetic field along the beam direction with a field strength of 0.5 T. The central barrel detectors, which cover the pseudorapidity interval $|\eta| < 0.9$, are the Inner Tracking System (ITS), the Time Projection Chamber (TPC), and the Time-Of-Flight (TOF) detectors, in order of radial distance from the beam axis. At midrapidity, the ITS and TPC provide track and vertex reconstruction. The TPC and TOF are used for particle identification (PID). At forward rapidity, the V0 detector assembly provides multiplicity estimation and triggering, with the V0A and V0C sub-detectors covering the pseudorapidity ranges $2.8 < \eta < 5.1$ and $-3.7 < \eta < -1.7$, respectively.

The data samples collected during the LHC Run 2 (2016, 2017, and 2018) from pp collisions at a centre-of-mass energy of $\sqrt{s} = 13$ TeV were used. During the data taking, two trigger conditions based on the signal amplitude recorded in the V0 detector were used. The minimum-bias (MB) trigger requires coincident signals in V0A and V0C at the same proton bunch crossing time. To enhance the selection of high-multiplicity events, a dedicated trigger, called the High Multiplicity V0 trigger (HMV0) was used. The HMV0 trigger condition

JHEP12(2025)038

Description	Trigger	Trigger efficiency ($\epsilon_{\text{trigger}}$)	Multiplicity class (p_{V0M} [%])	$\langle \mathrm{d}N_{\text{ch}}/\mathrm{d}\eta \rangle_{\lvert\eta\rvert<0.5}$
INEL $>$ 0	MB	0.920 $\pm$ 0.003	[0, 100]	6.93 $\pm$ 0.09
High multiplicity	HMV0	1 (negl. unc.)	[0, 0.1]	31.53 $\pm$ 0.38
Intermediate multiplicity	MB	0.997 $\pm$ 0.001	[0.1, 30]	13.81 $\pm$ 0.14
Low multiplicity	MB	0.897 $\pm$ 0.013	[30, 100]	4.41 $\pm$ 0.05

Table 2. Multiplicity classes based on p_{V0M} percentile and the corresponding $\langle \mathrm{d}N_{\text{ch}}/\mathrm{d}\eta \rangle_{\lvert\eta\rvert<0.5}$ [36, 43].

is satisfied if the sum of signal amplitude in V0A and V0C (denoted as V0M) is 5 times larger than the mean value in MB-triggered samples [36]. The trigger efficiencies are reported in table 2, as estimated in ref. [43].

Further offline event selections were applied to remove the contamination from beam-gas collisions and other machine-related backgrounds. These selection criteria were based on the signals from the V0 detector and the two innermost layers of the ITS, which constitute the Silicon Pixel Detector (SPD). Only events with a primary vertex within $\pm$10 cm of the nominal interaction point along the beam axis were selected. Moreover, events with multiple reconstructed primary vertices in the same proton bunch crossing (pile-up events) were excluded. In addition, a condition that requires at least one charged particle produced within the interval $|\eta| < 1$ (denoted as INEL $>$ 0) was applied to reject diffractive interactions. The events satisfying the aforementioned conditions account for about 75% of the total inelastic cross section [43, 44]. After the selections, the integrated luminosity of the analysed data sample was about $\mathcal{L}_{\text{int}} \approx 32\,\text{nb}^{-1}$ for the MB trigger and $\mathcal{L}_{\text{int}} \approx 7.7\,\text{pb}^{-1}$ for the HMV0 trigger [36].

The INEL $>$ 0 events were categorised into three classes based on the charged-particle multiplicity, which was estimated from the percentile distribution of V0M (p_{V0M}). Note that a small (large) value of p_{V0M} corresponds to high (low) charged-particle multiplicity. The p_{V0M} intervals were converted to the average charged-particle multiplicity in $|\eta| < 0.5$ ($\langle \mathrm{d}N_{\text{ch}}/\mathrm{d}\eta \rangle_{\lvert\eta\rvert<0.5}$), as explained in refs. [36, 43]. In table 2, the event classes and corresponding p_{V0M} intervals, along with the $\langle \mathrm{d}N_{\text{ch}}/\mathrm{d}\eta \rangle_{\lvert\eta\rvert<0.5}$ values, are summarised. The high-multiplicity (0–0.1%) events were collected with the HMV0 trigger, while the other multiplicity classes (0–100%, 0.1–30%, and 30–100%) were collected with the MB trigger.

3 Data analysis

In this article, Ξ_{c}^{+} and Ξ_{c}^{0} with their charge conjugates were analysed using hadronic decay channels ($\Xi_{\text{c}}^{+} \to \Xi^{-}\pi^{+}\pi^{+}$ and $\Xi_{\text{c}}^{0} \to \Xi^{-}\pi^{+}$) and a semileptonic decay channel ($\Xi_{\text{c}}^{0} \to \Xi^{-}\text{e}^{+}\nu_{\text{e}}$) at midrapidity ($|y| < 0.5$). The Ξ^{-} baryons appearing in these decay chains were reconstructed from $\Xi^{-} \to \Lambda\pi^{-}$, followed by $\Lambda \to \text{p}\pi^{-}$ [17]. In the analyses, Monte Carlo (MC) simulations with the PYTHIA 8 [45] event generator were used for various purposes, such as machine learning model training, acceptance-times-efficiency (Acc $\times$ ϵ) correction, unfolding, and template fit. The charm hadrons generated via PYTHIA 8 were forced to decay via the specific

JHEP12(2025)038

decay channel of interest in the analyses presented in this article. The interactions between the generated particles and the detectors were modelled using the GEANT3 package [46] and the detector geometry and conditions during the data taking were reproduced.

To reconstruct the $\Xi_c^{0,+}$ via their hadronic decay channels, a Ξ^- baryon candidate was paired with either one or two tracks, as described in refs. [11, 17]. The tracks were required to have at least 70 crossed pad rows in the TPC and at least 3 hits in the ITS. The identification of pions and protons was achieved by requiring the specific energy loss $\mathrm{d}E/\mathrm{d}x$ of the track and time-of-flight to be compatible with the expected values in units of the detector resolution (n_σ^{det}) within three standard deviations. Additional track quality selections were applied, as described in ref. [11]. Additionally, for Ξ_c^0 candidates, the Kalman Filter Particle tracking algorithm [47] was used to reconstruct the $\Xi_c^0 \to \Xi^-\pi^+$ decay channel.

A Boosted Decision Tree (BDT) algorithm, implemented using the XGBoost library [48] was adopted to separate the combinatorial background from the signal. The binary BDT classifiers were independently trained for each p_{T} interval with the sample extracted from the inclusive MB sample [5, 14, 19, 49]. The signal sample was obtained from MC simulations and the background sample was collected from data by selecting reconstructed $\Xi_c^{0,+}$ candidates located at least 6σ away from the invariant-mass signal peak, where σ corresponds to the width of the signal peak obtained from MC simulations. The BDT models were trained using variables related to PID and the decay topology of $\Xi_c^{0,+}$ baryons, such as the distance of closest approach (DCA) between the Ξ^- baryon and the pion coming from a $\Xi_c^{0,+}$ candidate, the DCA between the primary vertex and daughter particles, the pointing angle between the reconstructed momentum vector of $\Xi_c^{0,+}$ baryon and the vector that connects the primary and secondary vertices, and the reconstructed invariant mass of the Ξ and Λ. The output score from the trained BDT model allows each candidate to be classified with the probability of being a true signal. In each p_{T} interval, the threshold value of the BDT score was chosen to maximise the expected statistical significance of the signal, according to the procedure described in ref. [12]. The $\Xi_c^{0,+}$ signal was measured via a binned maximum-likelihood fit of the candidate invariant-mass distribution in each multiplicity class in the p_{T} intervals $4 < p_{\mathrm{T}} < 12$ GeV/c for Ξ_c^+ and $2 < p_{\mathrm{T}} < 12$ GeV/c for the Ξ_c^0. A Gaussian function was used to describe the signal, and its width (σ) was fixed to the value observed in MC simulations to improve the stability of the fit. The background was modelled with a first- or second-order polynomial, depending on the shape of the background in each p_{T} and multiplicity interval. The statistical significance of the obtained $\Xi_c^{0,+}$ signal ranged from 3.2σ to 8.4σ. Some examples of these fits are presented in figure 1.

For the Ξ_c^0 semileptonic decay, the Ξ_c^0 invariant mass cannot be fully reconstructed due to the presence of a neutrino in the decay chain, and the signal candidates were obtained by pairing an electron and a Ξ of opposite charges. Candidate electron tracks were selected by requiring at least three hits in the ITS with two in the SPD, a minimum of 50 reconstructed clusters and 70 crossed pad rows in the TPC, $p_{\mathrm{T}} > 0.5\,\mathrm{GeV}/c$, and identified with the TPC and TOF detectors by requiring selection criteria $\left|n_\sigma^{\mathrm{TPC}}\right| < 3$ and $\left|n_\sigma^{\mathrm{TOF}}\right| < 3$ [50]. The requirement for hits in both layers of the SPD was used to reject electrons from late photon conversions [51, 52]. Lastly, to suppress the electrons from Dalitz decays, each track was paired with opposite-sign tracks in the same event, and the track was discarded if it formed

JHEP12(2025)038

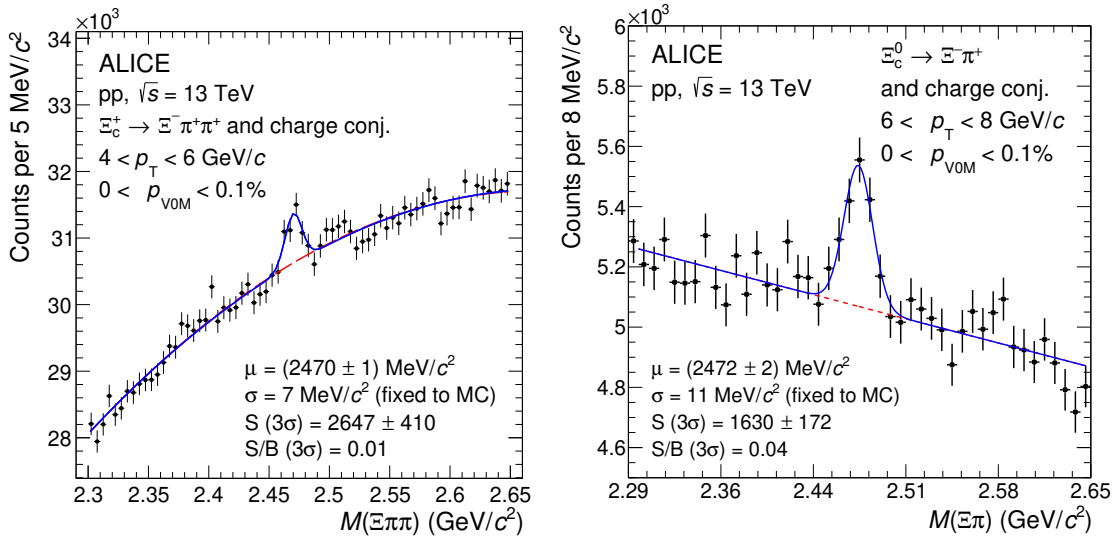

Figure 1. Invariant-mass distributions of signal candidates for the hadronic decays of Ξ_c^+ in $4 < p_T < 6\,\mathrm{GeV}/c$ (left), and Ξ_c^0 in $6 < p_T < 8\,\mathrm{GeV}/c$ (right), in the high-multiplicity class. The blue solid curve shows the total fit, and the red dashed curve shows the combinatorial background.

at least one pair with an invariant mass smaller than $50\,\mathrm{MeV}/c^2$ [18]. Once the eΞ pairs were built, they were required to be within $|y| < 0.5$ and have masses ($M_{e\Xi}$) larger than $1.3\,\mathrm{GeV}/c^2$. In addition, the pairs were filtered out by a criterion based on the opening angle between the electron and the Ξ momentum directions, which was obtained by studying the signal ($\Xi_c^0 \to \Xi^- e^+ \nu_e$) in MC. The criterion was determined by the angle at which 90% of eΞ pair yields remain and was tuned for each p_T interval in order to minimise the rejection of signal candidates in the data. The resulting values were distributed from 60° to 23°, decreasing with increasing p_T.

The selected eΞ pairs are composed of three different contributions: i) the pairs from $\Xi_c^0 \to \Xi^- e^+ \nu_e$ (signal); ii) the pairs from other decay channels $\Xi_c^0 \to e^+ \Xi^{*-} \nu_e \to e^+ (\Xi^- \pi^0) \nu_e$ and $\Xi_c^+ \to e^+ \Xi^{*0} \nu_e \to e^+ (\Xi^- \pi^+) \nu_e$, hereafter denoted as *4-body decay* background; and iii) combinatorial background. Since the difference between the $\Xi_c^0 \to \Xi^- e^+ \nu_e$ signal and 4-body decay background is only a soft pion from the resonance decay, the invariant-mass distribution of the 4-body decay background is slightly shifted towards lower masses with respect to the signal one, as shown in figure 2. To measure the reconstructed $\Xi_c^0 \to \Xi^- e^+ \nu_e$ yield, a corresponding template for each type of eΞ pair was prepared and used to fit the overall eΞ pair candidates. The sources of the template for each type of eΞ pair were as follows: i) $\Xi_c^0 \to \Xi^- e^+ \nu_e$ signal from MC; ii) 4-body decay background from MC; and iii) combinatorial background of eΞ pairs modelled with same-charge sign pairs from data [17]. Figure 2 shows examples of the template fit for the p_T interval $4 < p_T < 6$ GeV/c in the high- and low-multiplicity classes. In each panel, the distributions show the templates for each type of eΞ pair, and the total fit indicates the sum of the templates after the fit was performed. The reliability of the template fit method was validated by an MC closure test, which will be explained in section 4. Once the eΞ pairs from $\Xi_c^0 \to \Xi^- e^+ \nu_e$ were extracted, the p_T distribution of the pairs was corrected for the missing momentum carried by ν_e, using a Bayesian unfolding technique [53] implemented in the RooUnfold package [54].

JHEP12(2025)038

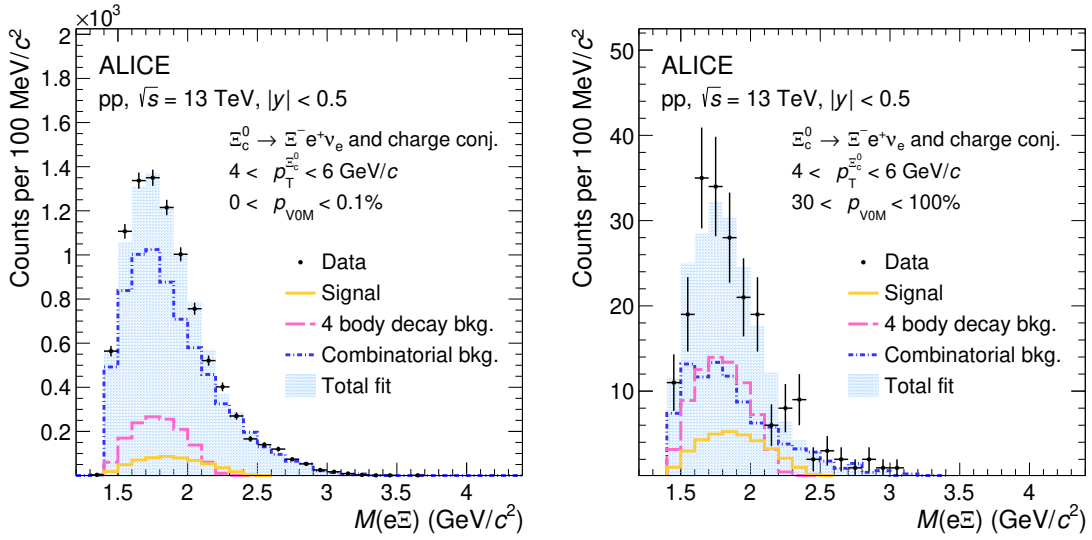

Figure 2. Invariant-mass distribution of eΞ pairs for $\Xi_c^0 \to \Xi^- e^+ \nu_e$ in $4 < p_T < 6\,\mathrm{GeV}/c$, in the high- (left) and low- (right) multiplicity classes. The blue filled distribution shows the total fit and the coloured lines indicate the different sources contributing to the fit.

The p_T-differential production yield of prompt $\Xi_c^{0,+}$ per event in each multiplicity class was calculated as

$$\frac{1}{N_{\mathrm{event}}} \frac{\mathrm{d}^2 N_{\mathrm{prompt}}^{\Xi_c^{0,+}}}{\mathrm{d}p_T\,\mathrm{d}y} = \frac{\epsilon_{\mathrm{trigger}}}{N_{\mathrm{event}}} \times \frac{1}{\mathrm{BR}} \times \frac{1}{2\Delta y \Delta p_T} \times \frac{f_{\mathrm{prompt}} \times N_{\mathrm{raw}}^{\Xi_c^{0,+}}}{(\mathrm{Acc} \times \epsilon)_{\mathrm{prompt}}}, \tag{3.1}$$

where N_{event} denotes the number of events in the corresponding multiplicity class, $\epsilon_{\mathrm{trigger}}$ is the trigger efficiency as reported in table 2, and BR represents the branching ratio of the considered decay channel. The factor of 2 accounts for the average yield of particles and antiparticles. Δy and Δp_T denote the rapidity coverage and the width of the p_T interval, respectively. f_{prompt} refers to the fraction of prompt $\Xi_c^{0,+}$ in the extracted raw yield, $N_{\mathrm{raw}}^{\Xi_c^{0,+}}$ is the raw yield (sum of particles and antiparticles), and $(\mathrm{Acc} \times \epsilon)_{\mathrm{prompt}}$ corresponds to the acceptance-times-efficiency for prompt $\Xi_c^{0,+}$ in the given multiplicity interval.

In the $(\mathrm{Acc} \times \epsilon)$ computation, the p_T distribution of $\Xi_c^{0,+}$ hadrons generated in MC simulations was tuned with an ad-hoc weight to better match the p_T distribution of the corrected data. To derive this weight, the ratio of the corrected yield of $\Xi_c^{0,+}$ in the analysed data to the generated $\Xi_c^{0,+}$ in MC was computed as a function of p_T. This p_T-dependent ratio was then fitted with an exponential function to obtain the weight. An additional weight was assigned to account for the multiplicity dependence of the $(\mathrm{Acc} \times \epsilon)$, which originates from the dependence of the primary-vertex resolution on the charged-particle multiplicity. The weight was defined as the ratio between the N_{tracklet} distribution measured in data and MC, where N_{tracklet} represents the number of track segments built by associating pairs of hits in the two layers of the SPD, which is proportional to the charged-particle multiplicity. The N_{tracklet} distributions from MC simulations were obtained by considering events with at least one $\Xi_c^{0,+}$ candidate, whose invariant mass lay within a specific range. For $\Xi_c^{0,+}$ hadronic decays, the range was based on the width of the signal peak obtained around the

JHEP12(2025)038

PDG mass [40]: ±20 MeV from the central position for $\Xi_c^0 \to \Xi^-\pi^+$ and ±30 MeV from the central position for $\Xi_c^+ \to \Xi^-\pi^+\pi^+$. For Ξ_c^0 semileptonic decays, the range was $M_{e\Xi} > 1.3$ GeV. The weighted efficiencies computed for the different multiplicity classes show a maximum of 5% variation with respect to those computed for the multiplicity-integrated sample for Ξ_c^0 baryons. However, for Ξ_c^+, a maximum 15% variation was observed in the high-multiplicity class, which decreased with increasing p_T.

The prompt fraction $f_{\rm prompt}$ in the total observed yield was estimated using a procedure similar to that described in ref. [17], to correct for the $\Xi_c^{0,+}$ yield originating from the beauty-hadron decays. In the estimation, it was assumed to be independent of the charged-particle multiplicity and therefore was obtained from the multiplicity-integrated event class ($0 < p_{\rm V0M} < 100\%$). This assumption is justified by the recent measurements of the non-prompt fraction of D mesons at midrapidity [55], where the ratio of the non-prompt fraction in different multiplicity classes to that in the multiplicity-integrated class was found to be compatible with unity [55]. The $f_{\rm prompt}$ was calculated as

$$f_{\rm prompt} = 1 - \frac{N^{\Xi_c^{0,+}}_{\rm non\text{-}prompt}}{N^{\Xi_c^{0,+}}_{\rm raw}} \tag{3.2}$$

$$= 1 - \frac{1}{N^{\Xi_c^{0,+}}_{\rm raw}} \times \left(\frac{{\rm d}^2\sigma}{{\rm d}p_T{\rm d}y}\right)^{\Xi_c^{0,+}}_{\rm non\text{-}prompt} \times {\rm BR} \times 2\Delta y \Delta p_T \times ({\rm Acc}\times\epsilon)_{\rm non\text{-}prompt} \times \mathcal{L}_{\rm int}, \tag{3.3}$$

where $N^{\Xi_c^{0,+}}_{\rm raw}$ and $N^{\Xi_c^{0,+}}_{\rm non\text{-}prompt}$ indicates the extracted raw yields and non-prompt yields, $\left(\frac{{\rm d}^2\sigma}{{\rm d}p_T{\rm d}y}\right)^{\Xi_c^{0,+}}_{\rm non\text{-}prompt}$ denotes the cross section of the non-prompt $\Xi_c^{0,+}$ baryons, BR is the branching ratio of the corresponding decay channel, factor 2 accounts for the cross section being the average of particles and antiparticles, Δy and Δp_T represent the rapidity coverage and the width of the p_T interval, respectively, $({\rm Acc}\times\epsilon)_{\rm non\text{-}prompt}$ indicates the acceptance-times-efficiency for non-prompt $\Xi_c^{0,+}$ baryons, and $\mathcal{L}_{\rm int}$ denotes the integrated luminosity. Since the production cross section of non-prompt $\Xi_c^{0,+}$ baryons has not been measured yet, it was estimated by scaling the non-prompt Λ_c^+ cross section, under the assumption that the p_T-differential cross section of non-prompt $\Xi_c^{0,+}$ has a similar shape to that of non-prompt Λ_c^+ as

$$\left(\frac{{\rm d}^2\sigma}{{\rm d}p_T{\rm d}y}\right)^{\Xi_c^{0,+}}_{\rm non\text{-}prompt} \approx \left(\frac{{\rm d}^2\sigma}{{\rm d}p_T{\rm d}y}\right)^{\Lambda_c^+}_{\rm non\text{-}prompt} \cdot \frac{\sum_{h_b} f({\rm b}\to h_b \to \Xi_c)}{\sum_{h_b} f({\rm b}\to h_b \to \Lambda_c)}, \tag{3.4}$$

where h_b indicates a beauty-hadron species and the sum runs on all beauty-hadron species. The cross section of non-prompt Λ_c^+ was estimated by combining the b-quark production cross section from FONLL calculations [25] with the fragmentation fraction of b-quarks decaying into beauty hadrons measured by LHCb experiment [27]. The kinematics of beauty hadrons decaying into Λ_c^+ were simulated using the PYTHIA 8 event generator. The obtained non-prompt Λ_c^+ cross section was scaled with the rightmost term of eq. (3.4), which represents the fragmentation fraction of non-prompt $\Xi_c^{0,+}$ to that of non-prompt Λ_c^+, in order to estimate the non-prompt $\Xi_c^{0,+}$ cross section. By considering that only Λ_b^0 and Ξ_b^- baryons contribute to the yields of non-prompt Λ_c^+ and $\Xi_c^{0,+}$ baryons, respectively, the ratio was approximated as

JHEP12(2025)038

Decay channel	$\Xi_c^+ \to \Xi^-\pi^+\pi^+$			$\Xi_c^0 \to \Xi^-\pi^+$				$\Xi_c^0 \to \Xi^-e^+\nu_e$			
p_T (GeV/c)	4–6	6–8	8–12	2–4	4–6	6–8	8–12	2–4	4–6	6–8	8–12
Raw yield	5%	5%	6%	6%	7%	8%	9%	21%	11%	10%	5%
MC p_T shape	1%	negl.	negl.	3%	1%	negl.	negl.	5%	2%	1%	2%
MC multiplicity	negl.	negl.	negl.	negl.	negl.	negl.	negl.	1%	1%	1%	2%
Prompt fraction	$^{+4}_{-6}$%	$^{+4}_{-6}$%	$^{+6}_{-7}$%	$^{+3}_{-2}$%	$^{+3}_{-2}$%	$^{+4}_{-3}$%	$^{+4}_{-3}$%	$^{+5}_{-1}$%	$^{+6}_{-1}$%	$^{+4}_{-1}$%	$^{+4}_{-3}$%
Efficiency correction	9%	11%	11%	6%	6%	6%	5%	7%	5%	6%	6%
Tracking	5%	5%	5%	5%	5%	5%	5%	5%	5%	5%	5%
Unfolding	—	—	—	—	—	—	—	1%	4%	3%	4%
$\|y\|$ variation	—	—	—	—	—	—	—	1%	1%	1%	1%
Total	13%	14%	15%	11%	10%	12%	12%	23%	15%	14%	12%
Branching ratio	44.3%			18.9%				23.1%			

Table 3. Systematic uncertainties on the corrected prompt yield for the multiplicity-integrated event class.

eq. (3.5). It was estimated by scaling the measured prompt $\Xi_c^{0,+}/\Lambda_c^+$ cross section ratio [16, 17] with the production yield ratio of non-prompt to prompt $\Xi_c^{0,+}/\Lambda_c^+$ predicted by PYTHIA 8 with CR Mode 2 tune. This approach relies on the assumption that the p_T-differential cross section ratio of non-prompt $\Xi_c^{0,+}/\Lambda_c^+$ has a similar shape to that of the prompt case.

$$\frac{\sum_{h_b} f(b \to h_b \to \Xi_c)}{\sum_{h_b} f(b \to h_b \to \Lambda_c)} = \frac{f(b \to \Xi_b \to \Xi_c)}{f(b \to \Lambda_b \to \Lambda_c)} = \left(\frac{\frac{b\to\Xi_c}{b\to\Lambda_c}}{\frac{c\to\Xi_c}{c\to\Lambda_c}}\right)_{\text{PYTHIA 8}} \cdot \frac{(d^2\sigma/dp_T dy)^{\Xi_c^{0,+}}_{\text{prompt}}}{(d^2\sigma/dp_T dy)^{\Lambda_c^+}_{\text{prompt}}} \quad (3.5)$$

The estimated prompt fraction ranges between 0.94 and 0.98.

4 Systematic uncertainties

Systematic uncertainties on the prompt $\Xi_c^{0,+}$ yield measurements were estimated for each p_T interval and multiplicity class. The sources of systematic uncertainty were those relative to the raw yield extraction, the MC p_T shape, the computation of the prompt fraction, the efficiency correction, the tracking efficiencies, the unfolding procedure, and the $|y|$ variation. The uncertainties estimated in the multiplicity-integrated event class ($0 < p_{V0M} < 100\%$) were reported in table 3, while those for other multiplicity classes were provided in appendix A. The magnitudes of the uncertainty contributions were independent of multiplicity. The tracking efficiency, the PID selection related to the efficiency correction, and the generated $\Xi_c^{0,+}$ p_T shape were correlated across different multiplicity intervals, while the others were not. The contribution related to the PID selection was included in the systematic uncertainty associated with the efficiency correction.

The approach adopted to estimate the systematic uncertainty related to the raw-yield extraction depends on the $\Xi_c^{0,+}$ decay channel. For the $\Xi_c^+ \to \Xi^-\pi^+\pi^+$ and $\Xi_c^0 \to \Xi^-\pi^+$ decays, the uncertainty was evaluated by repeating the fitting procedure to the invariant-mass distributions in each p_T and multiplicity class with various background modelling functions and fitting ranges. In addition, a bin-counting method was employed to test the sensitivity

JHEP12(2025)038

to the signal shape by following the approach used in ref. [12]. The signal function width was fixed to the value observed in MC simulations and a variation of 10% was also applied. The root-mean-square (RMS) of the raw yield distribution and the deviation of the mean of the distribution with respect to the raw yield obtained for the central case were evaluated, and their quadratic sum was assigned as a systematic uncertainty. The final assigned uncertainties range from 5% to 6% for Ξ_c^+ and from 6% to 9% for Ξ_c^0, depending on the p_T of the $\Xi_c^{0,+}$ baryon. For the $\Xi_c^0 \to \Xi^- e^+ \nu_e$ decay, the uncertainty was evaluated using an MC closure test. To test the reliability of the template fit method discussed in section 3, multiple pseudo-data samples with a known (true) signal yield were created, and then template fits were performed on these pseudo-data samples to check the difference between the true and the measured signal yield. To create a sample, each type of eΞ pair was randomly sampled from its base template, with the same number of candidates as in the data in each p_T interval, with the signal fraction varying from 5% to 25%. The systematic uncertainty was estimated as the deviation between the true signal yield and the measured signal yield $(1 - N_{\text{measured}}/N_{\text{true}})$. The final assigned uncertainties range from 5% to 21%.

To estimate the uncertainty associated with the p_T shape of the generated $\Xi_c^{0,+}$ baryons in MC simulations, the weighting factor described in section 3 was varied within the uncertainties of the ratio between the data and the MC. The maximum assigned systematic uncertainty was 5%.

In the MC, the multiplicity was estimated with the N_{tracklet} distribution, which was corrected using weights. The systematic uncertainties of these weights were calculated independently among the decay channels. For the $\Xi_c^{0,+}$ hadronic decay channels, the event selection criteria for determining the weights were tested by varying the invariant-mass window of $\Xi_c^{0,+}$ candidates with respect to the PDG mass [40] and by removing the mass window requirement. The resulting uncertainty was negligible except for Ξ_c^0 baryons with $p_T < 6\,\text{GeV}/c$ in the high-multiplicity class, where the uncertainty was found to be at maximum of 4%. For the semileptonic decay of Ξ_c^0, the weights were obtained from the events with Ξ_c^0 candidates (eΞ pairs) having a mass within the range $1.3 < M_{e\Xi} < 2.5\ \text{GeV}/c^2$. The uncertainty was 1–2% for most cases except in the high-multiplicity class, where the maximum assigned systematic uncertainty was 5%.

To estimate the uncertainty in the prompt $\Xi_c^{0,+}$ fraction correction described in eqs. (3.4) and (3.5), the following two ingredients were considered: i) the non-prompt Λ_c^+ cross section from FONLL predictions and ii) the ratio of the fractions of b quarks contributing to $\Xi_c^{0,+}$ and Λ_c^+ yields ($f(b \to \Xi_b \to \Xi_c)$ / $f(b \to \Lambda_b \to \Lambda_c)$), as done in ref. [17]. The uncertainties of the FONLL prediction were estimated by varying the b-quark mass, factorisation scale, and renormalisation scale as prescribed in ref. [25]. The uncertainty on the b-quark fractions feeding down to $\Xi_c^{0,+}$ and Λ_c^+ baryons was estimated by setting upper and lower bounds as follows. For the upper bound, only the measured prompt $\Xi_c^{0,+}/\Lambda_c^+$ production yield ratios were considered, without scaling the ratio of non-prompt to prompt Λ_c^+ and $\Xi_c^{0,+}$ yields predicted by PYTHIA 8, to account for the possible differences between the $\Xi_c^{0,+}/\Lambda_c^+$ and Ξ_b/Λ_b^0 ratios. For the lower bound, the Ξ_b/Λ_b^0 ratio measured by the LHCb Collaboration [27] was considered. Here it was assumed that the relative contribution of beauty-hadron decays to Ξ_c^0 and Ξ_c^+ in different multiplicity classes remains constant. The maximum resulting

JHEP12(2025)038

uncertainty was 4%. To estimate potential deviations of f_{prompt} from the value computed in the multiplicity-integrated event class, a similar methodology to that in ref. [36] was utilised. The variation as a function of multiplicity was computed using PYTHIA 8 simulations. The systematic uncertainty was evaluated considering the ratio between the non-prompt fraction in a given multiplicity class and that in INEL $>$ 0 events. The maximum uncertainty was 3%. The uncertainty of the prompt fraction was calculated by taking the quadratic sum of two sources. The maximum uncertainty was 7%.

The uncertainty related to the efficiency correction associated with the selection of the BDT classification score was estimated by repeating the analysis for different threshold values on the BDT scores to obtain the prompt $\Xi_{\mathrm{c}}^{0,+}$ yield. The uncertainty was estimated as the quadratic sum of the RMS of the corrected prompt $\Xi_{\mathrm{c}}^{0,+}$ yield distribution obtained from the variations and the shift in its mean with respect to the yield obtained with the default threshold value. These variations in threshold values were limited to trials with a $\Xi_{\mathrm{c}}^{0,+}$ signal that has a statistical significance of more than 3σ to be less sensitive to statistical fluctuations. The resulting uncertainties ranged from 9% to 11% for the $\Xi_{\mathrm{c}}^{+} \to \Xi^{-}\pi^{+}\pi^{+}$ decay, and from 5% to 6% for the $\Xi_{\mathrm{c}}^{0} \to \Xi^{-}\pi^{+}$ decay. For the $\Xi_{\mathrm{c}}^{0} \to \Xi^{-}\mathrm{e}^{+}\nu_{\mathrm{e}}$ decays, a set of variations of the selection criteria was considered for each variable, and the maximum deviation from the result obtained with respect to the default selection values was assigned as the uncertainty. The procedure was repeated for all selection variables and the final uncertainty was calculated as the quadratic sum of the uncertainties associated with each variable. The estimated uncertainties from these variations ranged from 5% to 7%.

The systematic uncertainty related to the track reconstruction efficiency can be influenced by the criteria related to the track quality selection and the probability of prolonging tracks from the TPC to the ITS (matching efficiency). The effect of the first source was evaluated by calculating the prompt yields of $\Xi_{\mathrm{c}}^{0,+}$ baryons with varied track selection criteria. The RMS of the calculated prompt yields was assigned as the systematic uncertainty. As a result, a uniform 5% uncertainty was assigned for all p_{T} intervals of interest. To estimate the contribution from the second source, the uncertainty in the matching efficiency of the pion (for hadronic $\Xi_{\mathrm{c}}^{0,+}$ decay channels) and the electron (for the semileptonic Ξ_{c}^{0} decay channel) in data and MC were compared. The per-track uncertainty on the matching efficiency was propagated to $\Xi_{\mathrm{c}}^{0,+}$ candidates by taking the decay kinematics into account. In this evaluation, only matching efficiencies of pions and electrons were considered since the prolongation of the tracks from the TPC to the ITS hits was not required for the tracks originating from the Ξ decay. The resulting uncertainty ranged from 1% to 2%.

For the semileptonic decay channel of Ξ_{c}^{0}, two additional sources were considered for the total systematic uncertainty. The first source was the unfolding procedure to compensate for the missing momentum carried by ν_{e}. To estimate the uncertainty of the procedure, both the algorithm (Bayesian and Singular Value Decomposition [56]) and the number of iterations (2−6) were varied. The estimated uncertainties ranged from 1% to 4%. The second source came from possible differences in the acceptance of eΞ pairs between the data and the MC. To estimate the uncertainty, the rapidity interval was varied between $|y| < 0.5$ and 0.8. The estimated uncertainties were uniform for all p_{T} intervals at 1%.

JHEP12(2025)038

The systematic uncertainties described above are assumed to be uncorrelated with one another. Therefore, the total systematic uncertainty was calculated as the quadratic sum of each source for each p_{T} and multiplicity class.

5 Results

The corrected prompt yields of the Ξ_{c}^{0} from both hadronic and semileptonic decay channels are consistent within the statistical and systematic uncertainties uncorrelated over the particle types. The following systematic uncertainty sources are considered uncorrelated: raw yield, MC p_{T} shape, efficiency correction, unfolding, $|y|$ variation, and branching ratio. To obtain a result with better precision, a weighted average of the two measurements was computed with weights defined as the inverse of the quadratic sum of the relative statistical and uncorrelated systematic uncertainties. Figure 3 shows the p_{T}-differential yields of prompt Ξ_{c}^{0} and Ξ_{c}^{+} baryons measured in $|y| < 0.5$ in the multiplicity-integrated class (INEL > 0) and in three different charged-particle multiplicity classes in pp collisions at $\sqrt{s} = 13\,\mathrm{TeV}$. The statistical and systematic uncertainties are reported as vertical bars and open boxes, respectively, and the uncertainties from the branching ratio are displayed as shaded boxes. The multiplicity classes are represented in terms of the average charged-particle densities at midrapidity, $\langle \mathrm{d}N_{\mathrm{ch}}/\mathrm{d}\eta \rangle_{|\eta|<0.5}$ values, as reported in table 2. The top left panel of figure 3 shows the average result between the Ξ_{c}^{0} measurements in the hadronic and semileptonic decay channels measured in $2 < p_{\mathrm{T}} < 12$ GeV/c and the top right panel shows Ξ_{c}^{+} measured in $4 < p_{\mathrm{T}} < 12$ GeV/c. The prompt Ξ_{c}^{0} yields measured in four multiplicity classes are compatible with those of Ξ_{c}^{+} baryons, as expected from isospin symmetry, and as was observed in the previous measurement [17]. The bottom panels of figure 3 show the ratios between the $\Xi_{\mathrm{c}}^{0,+}$ yield in a given multiplicity class and that obtained in INEL > 0 events. To calculate the ratio, the correlation of the uncertainty sources between the multiplicity classes and the INEL > 0 class was considered as follows: i) the high-multiplicity class trigger (HMV0) and MC multiplicity were treated as uncorrelated; ii) raw yield extraction and cut variations were assumed to be partially correlated, where the largest uncertainty was chosen as the final contribution to the total uncertainty; and iii) the other sources were considered as fully correlated. The observed hardening trend of the p_{T} spectrum is compatible with that reported for D mesons and Λ_{c}^{+} in ref. [36]. However, the current measurement precision does not allow one to exclude a smoother, or even negligible, evolution of the p_{T} distribution with multiplicity.

Figure 4 shows the baryon-to-meson ratios $\Xi_{\mathrm{c}}^{0,+}/\mathrm{D}^{0}$ and the baryon-to-baryon ratios $\Xi_{\mathrm{c}}^{0,+}/\Lambda_{\mathrm{c}}^{+}$ in the measured multiplicity classes. In each panel, the bars (open boxes) indicate the statistical (systematic) uncertainty, while the shaded boxes represent the branching ratio uncertainties. For the propagation of the systematic uncertainty, the following uncertainty sources were treated as uncorrelated over the different baryon and meson measurements: raw yield extraction, MC p_{T} shape, efficiency correction, unfolding, $|y|$ variation, and branching ratio. Both the $\Xi_{\mathrm{c}}^{0,+}/\mathrm{D}^{0}$ and $\Xi_{\mathrm{c}}^{0,+}/\Lambda_{\mathrm{c}}^{+}$ ratios measured in the INEL > 0 class are consistent with the measurements in ref. [17] within the uncertainties. The measured $\Xi_{\mathrm{c}}^{0,+}/\mathrm{D}^{0}$ ratios show no significant dependence on p_{T} within the current experimental uncertainties. The ratios measured in high-multiplicity classes are compatible with those measured in low-multiplicity classes. In contrast, the p_{T}-dependent $\Lambda_{\mathrm{c}}^{+}/\mathrm{D}^{0}$ ratio exhibits an increasing trend

JHEP12(2025)038

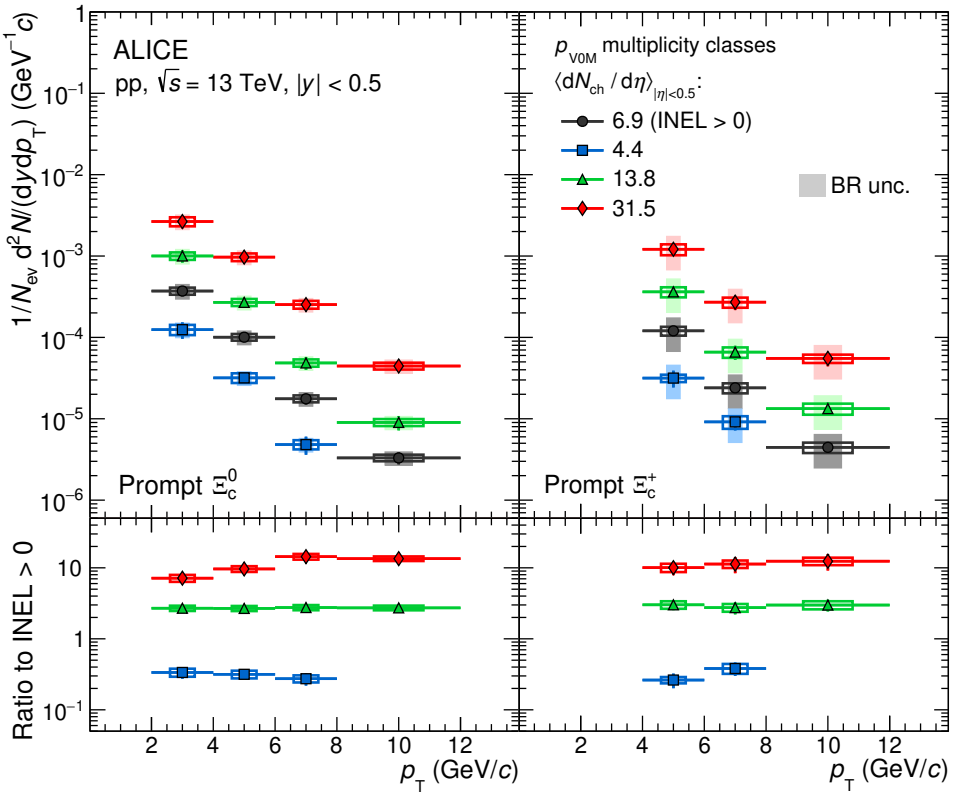

Figure 3. p_{T}-differential per-event yield of prompt Ξ_{c}^{0} (left) and Ξ_{c}^{+} (right) baryons measured in the different multiplicity classes in pp collisions at $\sqrt{s} = 13\,\mathrm{TeV}$ at midrapidity ($|y| < 0.5$), along with the corresponding ratios to the multiplicity-integrated (INEL > 0) class in the bottom panel. The values shown in the legend, denoted as $\langle \mathrm{d}N_{\mathrm{ch}}/\mathrm{d}\eta \rangle_{|\eta|<0.5}$, correspond to the average charged-particle multiplicity at midrapidity for the respective multiplicity classes, as introduced in table 2. The statistical and systematic uncertainties are shown as bars and open boxes, respectively. The shaded boxes indicate the uncertainty of the branching ratio.

with charged-particle multiplicity, indicating a possible modification of the hadronisation process in high-multiplicity environments [36]. Interestingly, however, the p_{T}-integrated $\Lambda_{\mathrm{c}}^{+}/\mathrm{D}^{0}$ ratio shows no significant dependence on multiplicity [36], similarly to the behaviour observed for the $\Lambda/\mathrm{K}_{\mathrm{S}}^{0}$ ratio, while the p_{T}-integrated $\Xi^{-}/\mathrm{K}_{\mathrm{S}}^{0}$ and $\Omega^{-}/\mathrm{K}_{\mathrm{S}}^{0}$ ratios increase with increasing charged-particle multiplicity [37].

Figure 5 shows the baryon-to-meson ratios $\Xi_{\mathrm{c}}^{0,+}/\mathrm{D}^{0}$ and baryon-to-baryon ratios $\Xi_{\mathrm{c}}^{0,+}/\Lambda_{\mathrm{c}}^{+}$ obtained from the low- and the high-multiplicity classes, compared with model calculations from the PYTHIA 8.2 [45] and the EPOS4HQ [57] event generators. Both the PYTHIA 8.2 and the EPOS4HQ predictions use the same multiplicity classes as the measurements. Note that both predictions are computed by considering Ξ_{c}^{0} only, however, the predictions for Ξ_{c}^{+} won't be significantly different being the isospin partner of Ξ_{c}^{0}. The PYTHIA 8.2 simulations are obtained by using the standard Monash 2013 tune and the colour reconnection settings beyond the leading colour approximation (CR-BLC) [30]. The CR-BLC modes used in this study (0, 2, and 3) apply different constraints on the allowed reconnection among colour sources, which leads to increased baryon production. In the EPOS4HQ, after the initial

JHEP12(2025)038

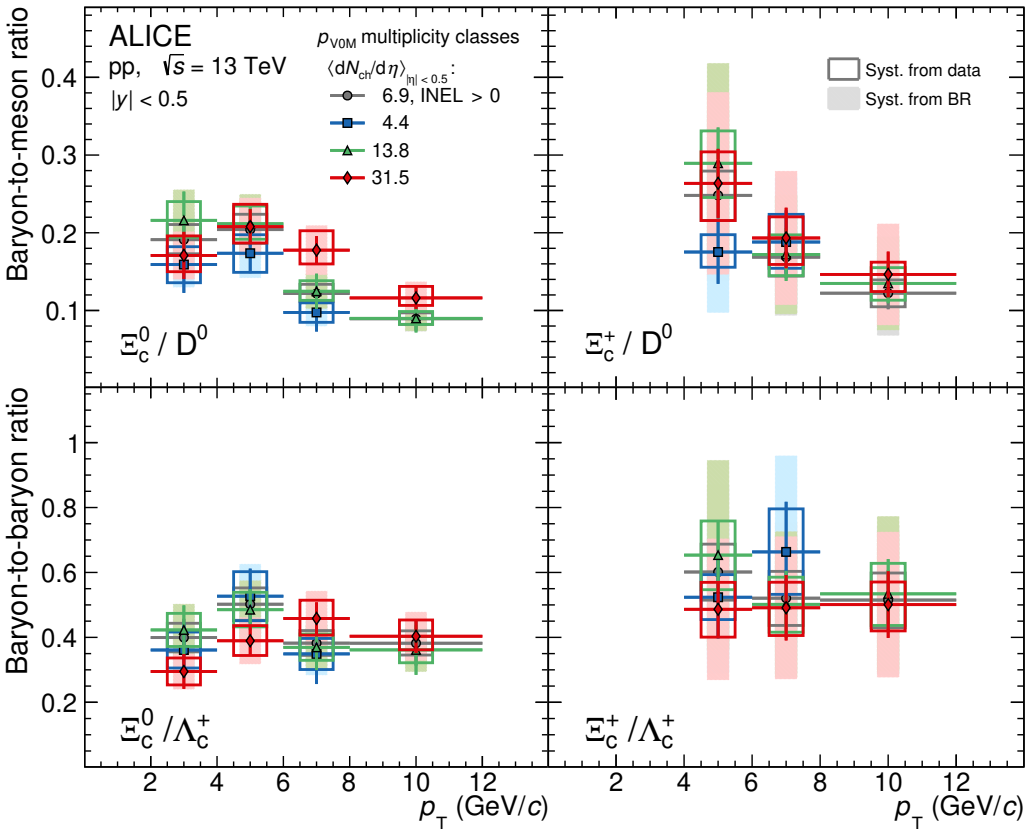

Figure 4. The prompt production yield ratios between $\Xi_c^{0,+}$ and D^0 mesons (top) and $\Xi_c^{0,+}$ and Λ_c^+ baryons (bottom) measured in the same multiplicity classes in pp collisions at $\sqrt{s} = 13$ TeV [36]. The statistical and systematic uncertainties are shown as bars and open boxes, and the uncertainty from BR is represented in shaded boxes, respectively.

parallel scatterings, the medium is separated into core and corona components, and then the evolution of the core is modelled using viscous hydrodynamics. Heavy quarks are produced initially via time-like cascades, space-like cascades, and Born processes. A heavy quark may enter the fluid, and propagate through the medium, interacting with thermal partons through elastic and inelastic scatterings, during which it can lose or gain energy. When the local energy density drops below a critical threshold, the heavy quark may hadronise into various heavy-flavour hadrons via a coalescence mechanism. In contrast, heavy quarks which do not enter the fluid hadronise always via fragmentation. The measured p_T-differential baryon-to-meson ratios and baryon-to-baryon ratios show no significant dependence on multiplicity with the current uncertainties. The predictions from PYTHIA 8.2 show no clear trend with multiplicity for Monash and CR-BLC mode 2. However, a slight increase can be observed for CR-BLC modes 0 and 3 in high multiplicity at low p_T. For both $\Xi_c^{0,+}/D^0$ and $\Xi_c^{0,+}/\Lambda_c^+$, both the Monash tune and the CR-BLC modes substantially underestimate the measured ratios in all multiplicity classes. On the other hand, the predictions from the EPOS4HQ show a relatively good description of the data. The predictions agree with the data both qualitatively and quantitatively considering the systematic uncertainty, especially at high multiplicity. It is also worth noting that the EPOS4HQ predictions show an evolution with

JHEP12(2025)038

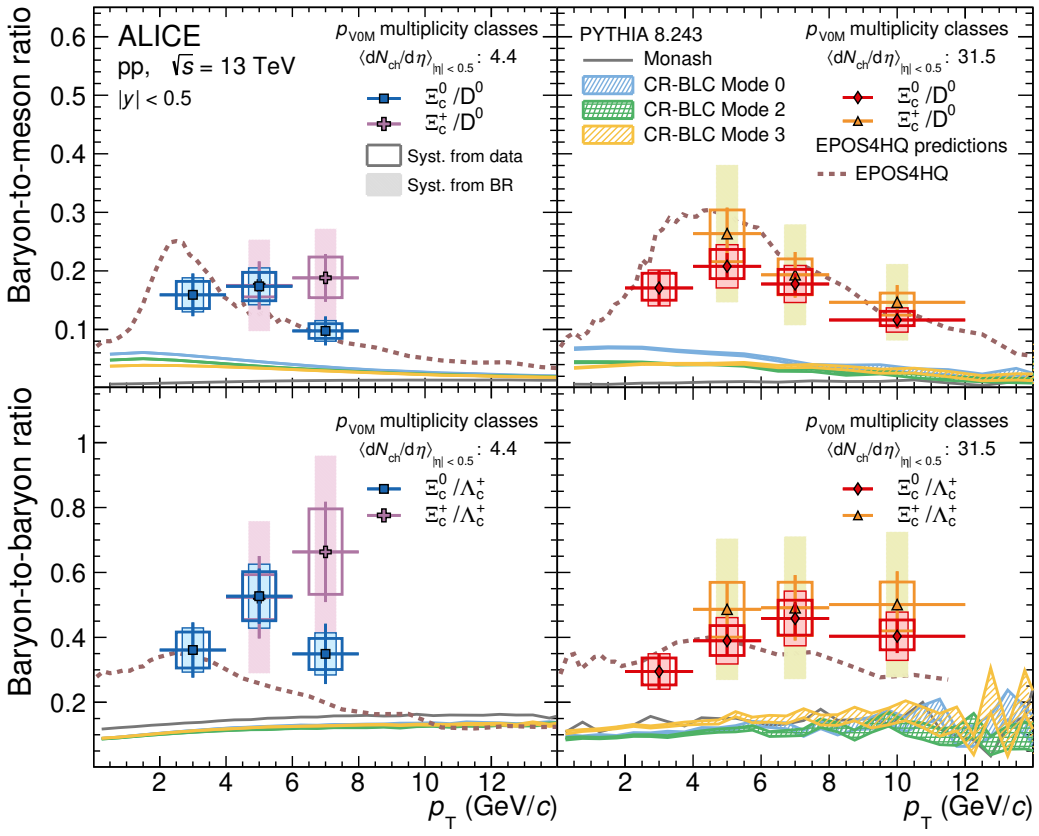

Figure 5. The baryon-to-meson ratios (top) and baryon-to-baryon ratios (bottom), measured in the low- (left) and high- (right) multiplicity classes. The measurements are compared with the predictions from two event generators: PYTHIA 8 with different tunes (namely Monash [26], CR-BLC [30] Mode 0, 2, and 3) and EPOS4HQ [57].

multiplicity. The main reason for this evolution is the fraction of charm quarks entering the fluid, since a fluid is created more frequently at high multiplicity and therefore has the chance to hadronise via coalescence, rather than via fragmentation. The latter strongly suppresses high masses compared to light ones, whereas the former only requires the presence of light quarks in the fluid to combine into charmed hadrons. The measurements of $\Xi_c^{0,+}$ production as a function of charged-particle multiplicity can put further constraints on the description of hadronisation mechanisms into baryons with charm and strange valence quarks. Aside from the Ξ_c^0/D^0 ratio in this analysis, note that the PYTHIA 8 CR-BLC modes have shown a significant multiplicity dependence in the Λ_c^+/D^0 ratio [36], especially for modes 0 and 2. In addition, they qualitatively describe the measured p_T-differential Λ_c^+/D^0 ratio, including the decreasing trend with p_T and the overall magnitude as a function of charged-particle multiplicity. Also, it is noteworthy that the PYTHIA 8 CR-BLC modes predict a dependence on the charged-particle multiplicity of the p_T-integrated Λ_c^+/D^0 ratio, which is not suggested by the experimental data [36].

Figure 6 shows the branching fraction ratio between the two considered decay channels of the Ξ_c^0 baryon $BR(\Xi_c^0 \to \Xi^- e^+ \nu_e)/BR(\Xi_c^0 \to \Xi^- \pi^+)$, compared with results from the ARGUS, Belle, and CLEO experiments [58–60] and theoretical predictions [61, 62]. To

JHEP12(2025)038

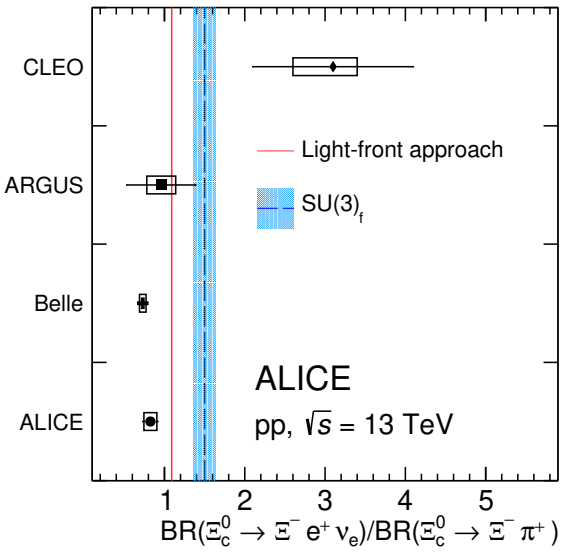

Figure 6. Comparison of $\mathrm{BR}(\Xi_c^0 \to \Xi^- e^+ \nu_e)/\mathrm{BR}(\Xi_c^0 \to \Xi^- \pi^+)$ between experiments [58–60] and model predictions [61, 62].

calculate the branching fraction ratio, the production yield ratio between the two Ξ_c^0 decay channels is obtained considering the (Acc $\times$ ϵ) corrected Ξ_c^0 yields in the two decay channels without correcting them by the respective branching ratios. The measured ratio does not show any significant p_T dependence. To provide a single value of the branching fraction ratio, the ratios in different p_T intervals were averaged by using the inverse of the sum in quadrature of the relative statistical and uncorrelated systematic uncertainties as weights as described in refs. [17, 50]. In the calculation, the following uncertainty sources are considered as p_T uncorrelated: the raw yield extraction (for both $\Xi_c^0 \to \Xi^- \pi^+$ and $\Xi_c^0 \to \Xi^- e^+ \nu_e$), the BDT efficiency correction for the hadronic decay channel, and the unfolding procedure for the semileptonic decay channel. The resulting branching fraction ratio is $\mathrm{BR}(\Xi_c^0 \to \Xi^- e^+ \nu_e)/\mathrm{BR}(\Xi_c^0 \to \Xi^- \pi^+) = 0.825 \pm 0.094$ (stat.) $\pm$ 0.081 (syst.). This result supersedes the previous ALICE measurement [17] with a factor 1.6 improvement in statistical precision, due to the inclusion of both MB and HMV0 triggered data samples. The branching fraction ratio is consistent with the Belle result [59] within 0.72σ. However, the values predicted by theoretical models such as the Light-front approach [61] and $\mathrm{SU(3)_f}$ [62] overestimate the measured ratio, as illustrated in figure 6. Also, it is an interesting point that the measured branching fraction ratio of Ξ_c^0 is similar to that of Ω_c^0 [50] within 0.80σ, as predicted by model calculations using the Light-front approach and SU(3)f.

6 Summary

The p_T-differential production yields of prompt Ξ_c^+ and Ξ_c^0 baryons at midrapidity ($|y| < 0.5$) as a function of charged-particle multiplicity, in the p_T interval $4 < p_T < 12$ GeV/c for Ξ_c^+ and $2 < p_T < 12$ GeV/c for Ξ_c^0, are reported. This study presents the first multiplicity-dependent measurement of $\Xi_c^{0,+}$ baryons in pp collisions at midrapidity. The production yields for the minimum-bias multiplicity class INEL > 0 are similar to the previously published result [17].

JHEP12(2025)038

No significant multiplicity dependence is observed in either $\Xi_c^{0,+}/D^0$ or $\Xi_c^{0,+}/\Lambda_c^+$ within uncertainties. The EPOS4HQ prediction accurately describes the $\Xi_c^{0,+}/D^0$ ratio as a function of p_T and multiplicity, while the PYTHIA 8.2 Monash 2013 tune and CR-BLC modes fail to capture any feature of the measurement. The branching fraction ratio $BR(\Xi_c^0 \to \Xi^- e^+ \nu_e)/BR(\Xi_c^0 \to \Xi^- \pi^+)$ is also measured, and it supersedes the previous measurement [17] with a factor of 1.6 improvement in the statistical precision. This new branching fraction ratio is compatible with the Belle result within 0.72σ. Lastly, the current measurement can be improved by exploiting the large data sample of pp collisions at $\sqrt{s} = 13.6$ TeV being collected during the Run 3 of the LHC by the ALICE experiment, which underwent a significant upgrade during the LHC Long Shutdown 2.

Acknowledgments

The ALICE Collaboration would like to thank all its engineers and technicians for their invaluable contributions to the construction of the experiment and the CERN accelerator teams for the outstanding performance of the LHC complex. The ALICE Collaboration gratefully acknowledges the resources and support provided by all Grid centres and the Worldwide LHC Computing Grid (WLCG) collaboration. The ALICE Collaboration acknowledges the following funding agencies for their support in building and running the ALICE detector: A. I. Alikhanyan National Science Laboratory (Yerevan Physics Institute) Foundation (ANSL), State Committee of Science and World Federation of Scientists (WFS), Armenia; Austrian Academy of Sciences, Austrian Science Fund (FWF): [M 2467-N36] and Nationalstiftung für Forschung, Technologie und Entwicklung, Austria; Ministry of Communications and High Technologies, National Nuclear Research Center, Azerbaijan; Rede Nacional de Física de Altas Energias (Renafae), Financiadora de Estudos e Projetos (Finep), Fundação de Amparo à Pesquisa do Estado de São Paulo (FAPESP) and The Sao Paulo Research Foundation (FAPESP), Brazil; Bulgarian Ministry of Education and Science, within the National Roadmap for Research Infrastructures 2020–2027 (object CERN), Bulgaria; Ministry of Education of China (MOEC), Ministry of Science & Technology of China (MSTC) and National Natural Science Foundation of China (NSFC), China; Ministry of Science and Education and Croatian Science Foundation, Croatia; Centro de Aplicaciones Tecnológicas y Desarrollo Nuclear (CEADEN), Cubaenergía, Cuba; Ministry of Education, Youth and Sports of the Czech Republic, Czech Republic; The Danish Council for Independent Research | Natural Sciences, the VILLUM FONDEN and Danish National Research Foundation (DNRF), Denmark; Helsinki Institute of Physics (HIP), Finland; Commissariat à l'Energie Atomique (CEA) and Institut National de Physique Nucléaire et de Physique des Particules (IN2P3) and Centre National de la Recherche Scientifique (CNRS), France; Bundesministerium für Bildung und Forschung (BMBF) and GSI Helmholtzzentrum für Schwerionenforschung GmbH, Germany; General Secretariat for Research and Technology, Ministry of Education, Research and Religions, Greece; National Research, Development and Innovation Office, Hungary; Department of Atomic Energy Government of India (DAE), Department of Science and Technology, Government of India (DST), University Grants Commission, Government of India (UGC) and Council of Scientific and Industrial Research (CSIR), India; National Research and Innovation Agency — BRIN, Indonesia; Istituto Nazionale di Fisica Nucleare (INFN), Italy; Japanese Ministry of Education, Culture, Sports, Science and Technology (MEXT) and Japan

JHEP12(2025)038

Society for the Promotion of Science (JSPS) KAKENHI, Japan; Consejo Nacional de Ciencia (CONACYT) y Tecnología, through Fondo de Cooperación Internacional en Ciencia y Tecnología (FONCICYT) and Dirección General de Asuntos del Personal Academico (DGAPA), Mexico; Nederlandse Organisatie voor Wetenschappelijk Onderzoek (NWO), Netherlands; The Research Council of Norway, Norway; Pontificia Universidad Católica del Perú, Peru; Ministry of Science and Higher Education, National Science Centre and WUT ID-UB, Poland; Korea Institute of Science and Technology Information and National Research Foundation of Korea (NRF), Republic of Korea; Ministry of Education and Scientific Research, Institute of Atomic Physics, Ministry of Research and Innovation and Institute of Atomic Physics and Universitatea Nationala de Stiinta si Tehnologie Politehnica Bucuresti, Romania; Ministerstvo skolstva, vyskumu, vyvoja a mladeze SR, Slovakia; National Research Foundation of South Africa, South Africa; Swedish Research Council (VR) and Knut & Alice Wallenberg Foundation (KAW), Sweden; European Organization for Nuclear Research, Switzerland; Suranaree University of Technology (SUT), National Science and Technology Development Agency (NSTDA) and National Science, Research and Innovation Fund (NSRF via PMU-B B05F650021), Thailand; Turkish Energy, Nuclear and Mineral Research Agency (TENMAK), Turkey; National Academy of Sciences of Ukraine, Ukraine; Science and Technology Facilities Council (STFC), United Kingdom; National Science Foundation of the United States of America (NSF) and United States Department of Energy, Office of Nuclear Physics (DOE NP), United States of America. In addition, individual groups or members have received support from: Czech Science Foundation (grant no. 23-07499S), Czech Republic; FORTE project, reg. no. CZ.02.01.01/00/22_008/0004632, Czech Republic, co-funded by the European Union, Czech Republic; European Research Council (grant no. 950692), European Union; Deutsche Forschungs Gemeinschaft (DFG, German Research Foundation) "Neutrinos and Dark Matter in Astro- and Particle Physics" (grant no. SFB 1258), Germany; ICSC — National Research Center for High Performance Computing, Big Data and Quantum Computing and FAIR — Future Artificial Intelligence Research, funded by the NextGenerationEU program (Italy).

JHEP12(2025)038

A Systematic uncertainties for other multiplicity classes

Decay channel	$\Xi_c^+ \to \Xi^-\pi^+\pi^+$			$\Xi_c^0 \to \Xi^-\pi^+$				$\Xi_c^0 \to \Xi^-e^+\nu_e$			
p_T (GeV/c)	4–6	6–8	8–12	2–4	4–6	6–8	8–12	2–4	4–6	6–8	8–12
Raw yield	5%	6%	6%	10%	10%	10%	9%	21%	11%	10%	5%
MC p_T shape	1%	negl.	negl.	3%	1%	negl.	negl.	5%	2%	2%	3%
MC multiplicity	negl.	negl.	negl.	4%	1%	negl.	negl.	5%	4%	2%	5%
Prompt fraction	$^{+4}_{-6}$%	$^{+4}_{-6}$%	$^{+6}_{-8}$%	$^{+3}_{-3}$%	$^{+3}_{-3}$%	$^{+4}_{-4}$%	$^{+4}_{-4}$%	$^{+1}_{0}$%	$^{+1}_{0}$%	$^{+4}_{0}$%	$^{+4}_{0}$%
Efficiency correction	12%	11%	6%	6%	6%	6%	6%	5%	5%	5%	5%
Tracking	5%	5%	5%	5%	5%	5%	5%	5%	5%	5%	5%
Unfolding	—	—	—	—	—	—	—	2%	2%	2%	1%
$\|y\|$ variation	—	—	—	—	—	—	—	1%	1%	1%	1%
Total	16%	15%	12%	14%	13%	13%	13%	23%	14%	13%	12%

Table 4. Systematic uncertainties on the corrected prompt yield measured in high-multiplicity class.

Decay channel	$\Xi_c^+ \to \Xi^-\pi^+\pi^+$			$\Xi_c^0 \to \Xi^-\pi^+$				$\Xi_c^0 \to \Xi^-e^+\nu_e$			
p_T (GeV/c)	4–6	6–8	8–12	2–4	4–6	6–8	8–12	2–4	4–6	6–8	8–12
Raw yield	6%	6%	6%	7%	8%	9%	10%	21%	11%	10%	5%
MC p_T shape	1%	negl.	negl.	3%	1%	negl.	negl.	5%	2%	1%	2%
MC multiplicity	negl.	negl.	negl.	negl.	negl.	negl.	negl.	1%	1%	1%	2%
Prompt fraction	$^{+4}_{-6}$%	$^{+4}_{-6}$%	$^{+6}_{-7}$%	$^{+3}_{-2}$%	$^{+3}_{-2}$%	$^{+4}_{-3}$%	$^{+4}_{-3}$%	$^{+5}_{-1}$%	$^{+6}_{-1}$%	$^{+4}_{-1}$%	$^{+4}_{-3}$%
Efficiency correction	11%	11%	12%	6%	6%	6%	6%	7%	6%	6%	6%
Tracking	5%	5%	5%	5%	5%	5%	5%	5%	5%	5%	5%
Unfolding	—	—	—	—	—	—	—	1%	4%	3%	4%
$\|y\|$ variation	—	—	—	—	—	—	—	1%	1%	1%	1%
Total	14%	15%	16%	11%	11%	12%	13%	23%	15%	14%	12%

Table 5. Systematic uncertainties on the corrected prompt yield measured in intermediate-multiplicity class.

Decay channel	$\Xi_c^+ \to \Xi^-\pi^+\pi^+$		$\Xi_c^0 \to \Xi^-\pi^+$			$\Xi_c^0 \to \Xi^-e^+\nu_e$		
p_T (GeV/c)	4–6	6–8	2–4	4–6	6–8	2–4	4–6	6–8
Raw yield	5%	8%	10%	10%	9%	21%	11%	10%
MC p_T shape	1%	negl.	3%	1%	negl.	5%	2%	1%
MC multiplicity	negl.	negl.	negl.	negl.	negl.	1%	1%	1%
Prompt fraction	$^{+4}_{-6}$%	$^{+4}_{-6}$%	$^{+3}_{-2}$%	$^{+3}_{-2}$%	$^{+4}_{-3}$%	$^{+5}_{-1}$%	$^{+6}_{-1}$%	$^{+4}_{-1}$%
Efficiency correction	6%	14%	10%	10%	10%	7%	6%	6%
Tracking	5%	5%	5%	5%	5%	5%	5%	5%
Unfolding	—	—	—	—	—	1%	4%	3%
$\|y\|$ variation	—	—	—	—	—	1%	1%	1%
Total	11%	18%	16%	15%	15%	23%	15%	14%

Table 6. Systematic uncertainties on the corrected prompt yield measured in low-multiplicity class.

Data Availability Statement. This manuscript has associated data in a HEPData repository at: https://www.hepdata.net/record/ins2960135.

Code Availability Statement. This manuscript has associated code/software in a data repository. The code/software used for the analysis is publicly available on the github repository, at the links https://github.com/alisw/AliRoot and https://github.com/alisw/AliPhysics/.

Open Access. This article is distributed under the terms of the Creative Commons Attribution License (CC-BY4.0), which permits any use, distribution and reproduction in any medium, provided the original author(s) and source are credited.

References

[1] J.C. Collins, D.E. Soper and G.F. Sterman, *Heavy Particle Production in High-Energy Hadron Collisions*, *Nucl. Phys. B* **263** (1986) 37 [INSPIRE].

JHEP12(2025)038

[2] E. Braaten, K.-M. Cheung, S. Fleming and T.C. Yuan, *Perturbative QCD fragmentation functions as a model for heavy quark fragmentation*, *Phys. Rev. D* **51** (1995) 4819 [hep-ph/9409316] [INSPIRE].

[3] ALICE collaboration, Λ_c^+ *production in pp collisions at* $\sqrt{s} = 7$ *TeV and in p-Pb collisions at* $\sqrt{s_{\rm NN}} = 5.02$ *TeV*, *JHEP* **04** (2018) 108 [arXiv:1712.09581] [INSPIRE].

[4] ALICE collaboration, *Measurement of* $\rm D^0$, $\rm D^+$, $\rm D^{*+}$ *and* $\rm D_s^+$ *production in pp collisions at* $\sqrt{s} = 5.02$ *TeV with ALICE*, *Eur. Phys. J. C* **79** (2019) 388 [arXiv:1901.07979] [INSPIRE].

[5] ALICE collaboration, *Measurement of beauty and charm production in pp collisions at* $\sqrt{s} = 5.02$ *TeV via non-prompt and prompt D mesons*, *JHEP* **05** (2021) 220 [arXiv:2102.13601] [INSPIRE].

[6] ATLAS collaboration, *Measurement of* $D^{*\pm}$, $D^{\pm}$ *and* $D_s^{\pm}$ *meson production cross sections in pp collisions at* $\sqrt{s} = 7$ *TeV with the ATLAS detector*, *Nucl. Phys. B* **907** (2016) 717 [arXiv:1512.02913] [INSPIRE].

[7] CMS collaboration, *Measurement of prompt open-charm production cross sections in proton-proton collisions at* $\sqrt{s} = 13$ *TeV*, *JHEP* **11** (2021) 225 [arXiv:2107.01476] [INSPIRE].

[8] LHCb collaboration, *Measurements of prompt charm production cross-sections in pp collisions at* $\sqrt{s} = 5$ *TeV*, *JHEP* **06** (2017) 147 [arXiv:1610.02230] [INSPIRE].

[9] LHCb collaboration, *Measurements of prompt charm production cross-sections in pp collisions at* $\sqrt{s} = 13$ *TeV*, *JHEP* **03** (2016) 159 [*Erratum ibid.* **09** (2016) 013] [arXiv:1510.01707] [INSPIRE].

[10] ALICE collaboration, *First measurement of* $\rm D_{s1}(1^+)(2536)^+$ *and* $\rm D_{s2}^*(2^+)(2573)^+$ *production in proton-proton collisions at* $\sqrt{s} = 13$ *TeV at the LHC*, *Phys. Rev. D* **111** (2025) 112005 [arXiv:2409.11938] [INSPIRE].

[11] ALICE collaboration, *Charm production and fragmentation fractions at midrapidity in pp collisions at* $\sqrt{s} = 13$ *TeV*, *JHEP* **12** (2023) 086 [arXiv:2308.04877] [INSPIRE].

[12] ALICE collaboration, Λ_c^+ *Production and Baryon-to-Meson Ratios in pp and p-Pb Collisions at* $\sqrt{s_{NN}} = 5.02$ *TeV at the LHC*, *Phys. Rev. Lett.* **127** (2021) 202301 [arXiv:2011.06078] [INSPIRE].

[13] ALICE collaboration, Λ_c^+ *production in pp and in p-Pb collisions at* $\sqrt{s_{NN}} = 5.02$ *TeV*, *Phys. Rev. C* **104** (2021) 054905 [arXiv:2011.06079] [INSPIRE].

[14] ALICE collaboration, *First measurement of* Λ_c^+ *production down to* $p_{\rm T} = 0$ *in pp and p-Pb collisions at* $\sqrt{s_{\rm NN}} = 5.02$ *TeV*, *Phys. Rev. C* **107** (2023) 064901 [arXiv:2211.14032] [INSPIRE].

[15] CMS collaboration, *Production of* Λ_c^+ *baryons in proton-proton and lead-lead collisions at* $\sqrt{s_{\rm NN}} = 5.02$ *TeV*, *Phys. Lett. B* **803** (2020) 135328 [arXiv:1906.03322] [INSPIRE].

[16] ALICE collaboration, *Measurement of Prompt* D^0, Λ_c^+, *and* $\Sigma_c^{0,++}(2455)$ *Production in Proton-Proton Collisions at* $\sqrt{s} = 13$ *TeV*, *Phys. Rev. Lett.* **128** (2022) 012001 [arXiv:2106.08278] [INSPIRE].

[17] ALICE collaboration, *Measurement of the Cross Sections of* Ξ_c^0 *and* Ξ_c^+ *Baryons and of the Branching-Fraction Ratio* $BR(\Xi_c^0 \to \Xi^- e^+ \nu_e)/BR(\Xi_c^0 \to \Xi^- \pi^+)$ *in pp collisions at 13 TeV*, *Phys. Rev. Lett.* **127** (2021) 272001 [*Erratum ibid.* **134** (2025) 179902] [arXiv:2105.05187] [INSPIRE].

[18] ALICE collaboration, *Measurement of the production cross section of prompt* $\Xi_{\rm c}^0$ *baryons at midrapidity in pp collisions at* $\sqrt{s} = 5.02$ *TeV*, *JHEP* **10** (2021) 159 [arXiv:2105.05616] [INSPIRE].

JHEP12(2025)038

[19] ALICE collaboration, *First measurement of Ω_c^0 production in pp collisions at $\sqrt{s} = 13$ TeV*, *Phys. Lett. B* **846** (2023) 137625 [arXiv:2205.13993] [INSPIRE].

[20] ALICE collaboration, *The ALICE experiment: a journey through QCD*, *Eur. Phys. J. C* **84** (2024) 813 [arXiv:2211.04384] [INSPIRE].

[21] G. Kramer and H. Spiesberger, *Study of heavy meson production in p-Pb collisions at $\sqrt{S} = 5.02$ TeV in the general-mass variable-flavour-number scheme*, *Nucl. Phys. B* **925** (2017) 415 [arXiv:1703.04754] [INSPIRE].

[22] I. Helenius and H. Paukkunen, *Revisiting the D-meson hadroproduction in general-mass variable flavour number scheme*, *JHEP* **05** (2018) 196 [arXiv:1804.03557] [INSPIRE].

[23] B.A. Kniehl, G. Kramer, I. Schienbein and H. Spiesberger, *$\Lambda_c^\pm$ production in pp collisions with a new fragmentation function*, *Phys. Rev. D* **101** (2020) 114021 [arXiv:2004.04213] [INSPIRE].

[24] M. Cacciari, M. Greco and P. Nason, *The p_T spectrum in heavy-flavour hadroproduction.*, *JHEP* **05** (1998) 007 [hep-ph/9803400] [INSPIRE].

[25] M. Cacciari et al., *Theoretical predictions for charm and bottom production at the LHC*, *JHEP* **10** (2012) 137 [arXiv:1205.6344] [INSPIRE].

[26] P. Skands, S. Carrazza and J. Rojo, *Tuning PYTHIA 8.1: the Monash 2013 Tune*, *Eur. Phys. J. C* **74** (2014) 3024 [arXiv:1404.5630] [INSPIRE].

[27] LHCb collaboration, *Measurement of b hadron fractions in 13 TeV pp collisions*, *Phys. Rev. D* **100** (2019) 031102 [arXiv:1902.06794] [INSPIRE].

[28] ALICE collaboration, *Study of flavor dependence of the baryon-to-meson ratio in proton-proton collisions at $\sqrt{s} = 13$ TeV*, *Phys. Rev. D* **108** (2023) 112003 [arXiv:2308.04873] [INSPIRE].

[29] ALICE collaboration, *Charm-quark fragmentation fractions and production cross section at midrapidity in pp collisions at the LHC*, *Phys. Rev. D* **105** (2022) L011103 [arXiv:2105.06335] [INSPIRE].

[30] J.R. Christiansen and P.Z. Skands, *String Formation Beyond Leading Colour*, *JHEP* **08** (2015) 003 [arXiv:1505.01681] [INSPIRE].

[31] M. He and R. Rapp, *Charm-Baryon Production in Proton-Proton Collisions*, *Phys. Lett. B* **795** (2019) 117 [arXiv:1902.08889] [INSPIRE].

[32] S. Plumari et al., *Charmed Hadrons from Coalescence plus Fragmentation in relativistic nucleus-nucleus collisions at RHIC and LHC*, *Eur. Phys. J. C* **78** (2018) 348 [arXiv:1712.00730] [INSPIRE].

[33] V. Minissale, S. Plumari and V. Greco, *Charm hadrons in pp collisions at LHC energy within a coalescence plus fragmentation approach*, *Phys. Lett. B* **821** (2021) 136622 [arXiv:2012.12001] [INSPIRE].

[34] J. Song, H.-H. Li and F.-L. Shao, *New feature of low p_T charm quark hadronization in pp collisions at $\sqrt{s} = 7$ TeV*, *Eur. Phys. J. C* **78** (2018) 344 [arXiv:1801.09402] [INSPIRE].

[35] A. Beraudo et al., *Heavy-flavor transport and hadronization in pp collisions*, *Phys. Rev. D* **109** (2024) L011501 [arXiv:2306.02152] [INSPIRE].

[36] ALICE collaboration, *Observation of a multiplicity dependence in the pT-differential charm baryon-to-meson ratios in proton–proton collisions at $\sqrt{s} = 13$ TeV*, *Phys. Lett. B* **829** (2022) 137065 [arXiv:2111.11948] [INSPIRE].

JHEP12(2025)038

[37] ALICE collaboration, *Multiplicity dependence of (multi-)strange hadron production in proton-proton collisions at* $\sqrt{s} = 13$ *TeV*, *Eur. Phys. J. C* **80** (2020) 167 [arXiv:1908.01861] [INSPIRE].

[38] V. Vovchenko, B. Dönigus and H. Stoecker, *Multiplicity dependence of light nuclei production at LHC energies in the canonical statistical model*, *Phys. Lett. B* **785** (2018) 171 [arXiv:1808.05245] [INSPIRE].

[39] BELLE collaboration, *First measurements of absolute branching fractions of the* Ξ_c^+ *baryon at Belle*, *Phys. Rev. D* **100** (2019) 031101 [arXiv:1904.12093] [INSPIRE].

[40] PARTICLE DATA GROUP collaboration, *Review of Particle Physics*, *PTEP* **2022** (2022) 083C01 [INSPIRE].

[41] ALICE collaboration, *The ALICE experiment at the CERN LHC*, 2008 *JINST* **3** S08002 [INSPIRE].

[42] ALICE collaboration, *Performance of the ALICE Experiment at the CERN LHC*, *Int. J. Mod. Phys. A* **29** (2014) 1430044 [arXiv:1402.4476] [INSPIRE].

[43] ALICE collaboration, *Pseudorapidity distributions of charged particles as a function of mid- and forward rapidity multiplicities in pp collisions at* $\sqrt{s} = 5.02$, 7 *and* 13 *TeV*, *Eur. Phys. J. C* **81** (2021) 630 [arXiv:2009.09434] [INSPIRE].

[44] ALICE collaboration, *Measurement of charm and beauty production at central rapidity versus charged-particle multiplicity in proton-proton collisions at* $\sqrt{s} = 7$ *TeV*, *JHEP* **09** (2015) 148 [arXiv:1505.00664] [INSPIRE].

[45] T. Sjöstrand et al., *An introduction to PYTHIA 8.2*, *Comput. Phys. Commun.* **191** (2015) 159 [arXiv:1410.3012] [INSPIRE].

[46] R. Brun et al., *GEANT Detector Description and Simulation Tool*, CERN-W5013 CERN, Geneva (1994) [DOI:10.17181/CERN.MUHF.DMJ1] [INSPIRE].

[47] I. Kisel, I. Kulakov and M. Zyzak, *Standalone first level event selection package for the CBM experiment*, in the proceedings of the *18th Real-Time Conference*, Berkley, U.S.A. (2012) [DOI:10.1109/RTC.2012.6418385] [INSPIRE].

[48] T. Chen and C. Guestrin, *XGBoost: A Scalable Tree Boosting System*, arXiv:1603.02754 [DOI:10.1145/2939672.2939785] [INSPIRE].

[49] ALICE collaboration, *Measurement of prompt* D_s^+*-meson production and azimuthal anisotropy in Pb-Pb collisions at* $\sqrt{s_{NN}} = 5.02$ *TeV*, *Phys. Lett. B* **827** (2022) 136986 [arXiv:2110.10006] [INSPIRE].

[50] ALICE collaboration, *Measurement of* Ω_c^0 *baryon production and branching-fraction ratio* $\mathrm{BR}(\Omega_c^0 \to \Omega^- \mathrm{e}^+ \nu_e)/\mathrm{BR}(\Omega_c^0 \to \Omega^- \pi^+)$ *in pp collisions at* $\sqrt{s} = 13$ *TeV*, *Phys. Rev. D* **110** (2024) 032014 [arXiv:2404.17272] [INSPIRE].

[51] ALICE collaboration, *Measurements of low-*p_T *electrons from semileptonic heavy-flavour hadron decays at mid-rapidity in pp and Pb-Pb collisions at* $\sqrt{s_{\mathrm{NN}}} = 2.76$ *TeV*, *JHEP* **10** (2018) 061 [arXiv:1805.04379] [INSPIRE].

[52] ALICE collaboration, *Measurement of electrons from semileptonic heavy-flavour hadron decays at midrapidity in pp and Pb-Pb collisions at* $\sqrt{s_{\mathrm{NN}}} = 5.02$ *TeV*, *Phys. Lett. B* **804** (2020) 135377 [arXiv:1910.09110] [INSPIRE].

[53] G. D'Agostini, *A Multidimensional unfolding method based on Bayes' theorem*, *Nucl. Instrum. Meth. A* **362** (1995) 487 [INSPIRE].

JHEP12(2025)038

[54] T. Adye, *Unfolding algorithms and tests using RooUnfold*, in the proceedings of the *PHYSTAT 2011*, Geneva, Switzerland (2011) [DOI:10.5170/CERN-2011-006.313] [arXiv:1105.1160] [INSPIRE].

[55] ALICE collaboration, *Measurement of the non-prompt D-meson fraction as a function of multiplicity in proton-proton collisions at* $\sqrt{s} = 13$ *TeV*, *JHEP* **10** (2023) 092 [arXiv:2302.07783] [INSPIRE].

[56] A. Hocker and V. Kartvelishvili, *SVD approach to data unfolding*, *Nucl. Instrum. Meth. A* **372** (1996) 469 [hep-ph/9509307] [INSPIRE].

[57] J. Zhao et al., *Heavy-flavor hadron production in relativistic heavy ion collisions at energies available at BNL RHIC and at the CERN LHC in the EPOS4HQ framework*, *Phys. Rev. C* **110** (2024) 024909 [arXiv:2401.17096] [INSPIRE].

[58] ARGUS collaboration, *Observation of* Ξ_c^0 *semileptonic decay*, *Phys. Lett. B* **303** (1993) 368 [INSPIRE].

[59] BELLE collaboration, *Measurements of the branching fractions of the semileptonic decays* $\Xi_c^0 \to \Xi^- \ell^+ \nu_\ell$ *and the asymmetry parameter of* $\Xi_c^0 \to \Xi^- \pi^+$, *Phys. Rev. Lett.* **127** (2021) 121803 [arXiv:2103.06496] [INSPIRE].

[60] CLEO collaboration, *First observation of Decay* $\Xi_c^+ \to \Xi^0 e^+ \nu_e$ *and an Estimate of the* Ξ_c^+ Ξ_c^0 *lifetime ratio*, *Phys. Rev. Lett.* **74** (1995) 3113 [*Erratum ibid.* **75** (1995) 4155] [INSPIRE].

[61] Z.-X. Zhao, *Weak decays of heavy baryons in the light-front approach*, *Chin. Phys. C* **42** (2018) 093101 [arXiv:1803.02292] [INSPIRE].

[62] C.-Q. Geng, C.-W. Liu, T.-H. Tsai and S.-W. Yeh, *Semileptonic decays of anti-triplet charmed baryons*, *Phys. Lett. B* **792** (2019) 214 [arXiv:1901.05610] [INSPIRE].

JHEP12(2025)038

The ALICE collaboration

I.J. Abualrob[114], S. Acharya[50], G. Aglieri Rinella[32], L. Aglietta[24], M. Agnello[29], N. Agrawal[25], Z. Ahammed[133], S. Ahmad[15], I. Ahuja[36], ZUL. Akbar[81], A. Akindinov[139], V. Akishina[38], M. Al-Turany[96], D. Aleksandrov[139], B. Alessandro[56], H.M. Alfanda[6], R. Alfaro Molina[67], B. Ali[15], A. Alici[25], A. Alkin[103], J. Alme[20], G. Alocco[24], T. Alt[64], A.R. Altamura[50], I. Altsybeev[94], C. Andrei[45], N. Andreou[113], A. Andronic[124], E. Andronov[139], V. Anguelov[93], F. Antinori[54], P. Antonioli[51], N. Apadula[73], H. Appelshäuser[64], S. Arcelli[25], R. Arnaldi[56], J.G.M.C.A. Arneiro[109], I.C. Arsene[19], M. Arslandok[136], A. Augustinus[32], R. Averbeck[96], M.D. Azmi[15], H. Baba[122], A.R.J. Babu[135], A. Badalà[53], J. Bae[103], Y. Bae[103], Y.W. Baek[40], X. Bai[118], R. Bailhache[64], Y. Bailung[48], R. Bala[90], A. Baldisseri[128], B. Balis[2], S. Bangalia[116], Z. Banoo[90], V. Barbasova[36], F. Barile[31], L. Barioglio[56], M. Barlou[24,77], B. Barman[41], G.G. Barnaföldi[46], L.S. Barnby[113], E. Barreau[102], V. Barret[125], L. Barreto[109], K. Barth[32], E. Bartsch[64], N. Bastid[125], G. Batigne[102], D. Battistini[94], B. Batyunya[140], D. Bauri[47], J.L. Bazo Alba[100], I.G. Bearden[82], P. Becht[96], D. Behera[48], S. Behera[47], I. Belikov[127], V.D. Bella[127], F. Bellini[25], R. Bellwied[114], L.G.E. Beltran[108], Y.A.V. Beltran[44], G. Bencedi[46], A. Bensaoula[114], S. Beole[24], Y. Berdnikov[139], A. Berdnikova[93], L. Bergmann[73,93], L. Bernardinis[23], L. Betev[32], P.P. Bhaduri[133], T. Bhalla[89], A. Bhasin[90], B. Bhattacharjee[41], S. Bhattarai[116], L. Bianchi[24], J. Bielčík[34], J. Bielčíková[85], A. Bilandzic[94], A. Binoy[116], G. Biro[46], S. Biswas[4], D. Blau[139], M.B. Blidaru[96], N. Bluhme[38], C. Blume[64], F. Bock[86], T. Bodova[20], J. Bok[16], L. Boldizsár[46], M. Bombara[36], P.M. Bond[32], G. Bonomi[132,55], H. Borel[128], A. Borissov[139], A.G. Borquez Carcamo[93], E. Botta[24], Y.E.M. Bouziani[64], D.C. Brandibur[63], L. Bratrud[64], P. Braun-Munzinger[96], M. Bregant[109], M. Broz[34], G.E. Bruno[95,31], V.D. Buchakchiev[35], M.D. Buckland[84], H. Buesching[64], S. Bufalino[29], P. Buhler[101], N. Burmasov[140], Z. Buthelezi[68,121], A. Bylinkin[20], C. Carr[99], J.C. Cabanillas Noris[108], M.F.T. Cabrera[114], H. Caines[136], A. Caliva[28], E. Calvo Villar[100], J.M.M. Camacho[108], P. Camerini[23], M.T. Camerlingo[50], F.D.M. Canedo[109], S. Cannito[23], S.L. Cantway[136], M. Carabas[112], F. Carnesecchi[32], L.A.D. Carvalho[109], J. Castillo Castellanos[128], M. Castoldi[32], F. Catalano[32], S. Cattaruzzi[23], R. Cerri[24], I. Chakaberia[73], P. Chakraborty[134], J.W.O. Chan[114], S. Chandra[133], S. Chapeland[32], M. Chartier[117], S. Chattopadhay[133], M. Chen[39], T. Cheng[6], C. Cheshkov[126], D. Chiappara[27], V. Chibante Barroso[32], D.D. Chinellato[101], F. Chinu[24], E.S. Chizzali[II,94], J. Cho[58], S. Cho[58], P. Chochula[32], Z.A. Chochulska[III,134], P. Christakoglou[83], C.H. Christensen[82], P. Christiansen[74], T. Chujo[123], M. Ciacco[29], C. Cicalo[52], G. Cimador[24], F. Cindolo[51], G. Clai[IV,51], F. Colamaria[50], D. Colella[31], A. Colelli[31], M. Colocci[25], M. Concas[32], G. Conesa Balbastre[72], Z. Conesa del Valle[129], G. Contin[23], J.G. Contreras[34], M.L. Coquet[102], P. Cortese[131,56], M.R. Cosentino[111], F. Costa[32], S. Costanza[21], P. Crochet[125], M.M. Czarnynoga[134], A. Dainese[54], G. Dange[38], M.C. Danisch[93], A. Danu[63], P. Das[32], S. Das[4], A.R. Dash[124], S. Dash[47], A. De Caro[28], G. de Cataldo[50], J. de Cuveland[38], A. De Falco[22], D. De Gruttola[28], N. De Marco[56], C. De Martin[23], S. De Pasquale[28], R. Deb[132], R. Del Grande[94], L. Dello Stritto[32], G.G.A. de Souza[V,109], P. Dhankher[18], D. Di Bari[31], M. Di Costanzo[29],

JHEP12(2025)038

A. Di Mauro[32], B. Di Ruzza[130], B. Diab[32], Y. Ding[6], J. Ditzel[64], R. Divià[32], A. Dobrin[63], B. Dönigus[64], L. Döpper[42], J.M. Dubinski[134], A. Dubla[96], P. Dupieux[125], N. Dzalaiova[13], T.M. Eder[124], R.J. Ehlers[73], F. Eisenhut[64], R. Ejima[91], D. Elia[50], B. Erazmus[102], F. Ercolessi[25], B. Espagnon[129], G. Eulisse[32], D. Evans[99], L. Fabbietti[94], M. Faggin[32], J. Faivre[72], F. Fan[6], W. Fan[73], T. Fang[6], A. Fantoni[49], M. Fasel[86], A. Feliciello[56], G. Feofilov[139], A. Fernández Téllez[44], L. Ferrandi[109], M.B. Ferrer[32], A. Ferrero[128], C. Ferrero[VI,56], A. Ferretti[24], V.J.G. Feuillard[93], D. Finogeev[140], F.M. Fionda[52], A.N. Flores[107], S. Foertsch[68], I. Fokin[93], S. Fokin[139], U. Follo[VI,56], R. Forynski[113], E. Fragiacomo[57], E. Frajna[46], H. Fribert[94], U. Fuchs[32], N. Funicello[28], C. Furget[72], A. Furs[140], T. Fusayasu[97], J.J. Gaardhøje[82], M. Gagliardi[24], A.M. Gago[100], T. Gahlaut[47], C.D. Galvan[108], S. Gami[79], P. Ganoti[77], C. Garabatos[96], J.M. Garcia[44], T. García Chávez[44], E. Garcia-Solis[9], S. Garetti[129], C. Gargiulo[32], P. Gasik[96], H.M. Gaur[38], A. Gautam[116], M.B. Gay Ducati[66], M. Germain[102], R.A. Gernhaeuser[94], C. Ghosh[133], M. Giacalone[51], G. Gioachin[29], S.K. Giri[133], P. Giubellino[56], P. Giubilato[27], P. Glässel[93], E. Glimos[120], V. Gonzalez[135], M. Gorgon[2], K. Goswami[48], S. Gotovac[33], V. Grabski[67], L.K. Graczykowski[134], E. Grecka[85], A. Grelli[59], C. Grigoras[32], V. Grigoriev[139], S. Grigoryan[140,1], O.S. Groettvik[32], F. Grosa[32], J.F. Grosse-Oetringhaus[32], R. Grosso[96], D. Grund[34], N.A. Grunwald[93], R. Guernane[72], M. Guilbaud[102], K. Gulbrandsen[82], J.K. Gumprecht[101], T. Gündem[64], T. Gunji[122], J. Guo[10], W. Guo[6], A. Gupta[90], R. Gupta[90], R. Gupta[48], K. Gwizdziel[134], L. Gyulai[46], C. Hadjidakis[129], F.U. Haider[90], S. Haidlova[34], M. Haldar[4], H. Hamagaki[75], Y. Han[138], B.G. Hanley[135], R. Hannigan[107], J. Hansen[74], J.W. Harris[136], A. Harton[9], M.V. Hartung[64], A. Hasan[119], H. Hassan[115], D. Hatzifotiadou[51], P. Hauer[42], L.B. Havener[136], E. Hellbär[32], H. Helstrup[37], M. Hemmer[64], T. Herman[34], S.G. Hernandez[114], G. Herrera Corral[8], K.F. Hetland[37], B. Heybeck[64], H. Hillemanns[32], B. Hippolyte[127], I.P.M. Hobus[83], F.W. Hoffmann[38], B. Hofman[59], M. Horst[94], A. Horzyk[2], Y. Hou[96,11,6], P. Hristov[32], P. Huhn[64], L.M. Huhta[115], T.J. Humanic[87], V. Humlova[34], A. Hutson[114], D. Hutter[38], M.C. Hwang[18], R. Ilkaev[139], M. Inaba[123], M. Ippolitov[139], A. Isakov[83], T. Isidori[116], M.S. Islam[47], M. Ivanov[13], M. Ivanov[96], K.E. Iversen[74], J.G.Kim[138], M. Jablonski[2], B. Jacak[18,73], N. Jacazio[25], P.M. Jacobs[73], S. Jadlovska[105], J. Jadlovsky[105], S. Jaelani[81], C. Jahnke[110], M.J. Jakubowska[134], E.P. Jamro[2], D.M. Janik[34], M.A. Janik[134], S. Ji[16], S. Jia[82], T. Jiang[10], A.A.P. Jimenez[65], S. Jin[10], F. Jonas[73], D.M. Jones[117], J.M. Jowett[32,96], J. Jung[64], M. Jung[64], A. Junique[32], A. Jusko[99], J. Kaewjai[104], P. Kalinak[60], A. Kalweit[32], A. Karasu Uysal[137], N. Karatzenis[99], O. Karavichev[139], T. Karavicheva[139], M.J. Karwowska[134], U. Kebschull[70], M. Keil[32], B. Ketzer[42], J. Keul[64], S.S. Khade[48], A.M. Khan[118], A. Khanzadeev[139], Y. Kharlov[139], A. Khatun[116], A. Khuntia[51], Z. Khuranova[64], B. Kileng[37], B. Kim[103], C. Kim[16], D.J. Kim[115], D. Kim[103], E.J. Kim[69], G. Kim[58], H. Kim[58], J. Kim[138], J. Kim[58], J. Kim[32], M. Kim[18], S. Kim[17], T. Kim[138], K. Kimura[91], S. Kirsch[64], I. Kisel[38], S. Kiselev[139], A. Kisiel[134], J.L. Klay[5], J. Klein[32], S. Klein[73], C. Klein-Bösing[124], M. Kleiner[64], A. Kluge[32], C. Kobdaj[104], R. Kohara[122], T. Kollegger[96], A. Kondratyev[140], N. Kondratyeva[139], J. Konig[64], P.J. Konopka[32], G. Kornakov[134], M. Korwieser[94], S.D. Koryciak[2], C. Koster[83], A. Kotliarov[85],

JHEP12(2025)038

N. Kovacic[88], V. Kovalenko[139], M. Kowalski[106], V. Kozhuharov[35], G. Kozlov[38], I. Králik[60], A. Kravčáková[36], L. Krcal[32], M. Krivda[99,60], F. Krizek[85], K. Krizkova Gajdosova[34], C. Krug[66], M. Krüger[64], E. Kryshen[139], V. Kučera[58], C. Kuhn[127], T. Kumaoka[123], D. Kumar[133], L. Kumar[89], N. Kumar[89], S. Kumar[50], S. Kundu[32], M. Kuo[123], P. Kurashvili[78], A.B. Kurepin[139], S. Kurita[91], A. Kuryakin[139], S. Kushpil[85], M. Kutyla[134], A. Kuznetsov[140], M.J. Kweon[58], Y. Kwon[138], S.L. La Pointe[38], P. La Rocca[26], A. Lakrathok[104], M. Lamanna[32], S. Lambert[102], A.R. Landou[72], R. Langoy[119], E. Laudi[32], L. Lautner[94], R.A.N. Laveaga[108], R. Lavicka[101], R. Lea[132,55], H. Lee[103], I. Legrand[45], G. Legras[124], A.M. Lejeune[34], T.M. Lelek[2], I. León Monzón[108], M.M. Lesch[94], P. Lévai[46], M. Li[6], P. Li[10], X. Li[10], B.E. Liang-Gilman[18], J. Lien[119], R. Lietava[99], I. Likmeta[114], B. Lim[56], H. Lim[16], S.H. Lim[16], S. Lin[10], V. Lindenstruth[38], C. Lippmann[96], D. Liskova[105], D.H. Liu[6], J. Liu[117], G.S.S. Liveraro[110], I.M. Lofnes[20], C. Loizides[86], S. Lokos[106], J. Lömker[59], X. Lopez[125], E. López Torres[7], C. Lotteau[126], P. Lu[96,118], W. Lu[6], Z. Lu[10], F.V. Lugo[67], J. Luo[39], G. Luparello[57], M.A.T. Johnson[44], Y.G. Ma[39], M. Mager[32], A. Maire[127], E.M. Majerz[2], M.V. Makariev[35], G. Malfattore[51], N.M. Malik[90], N. Malik[15], S.K. Malik[90], D. Mallick[129], N. Mallick[115], G. Mandaglio[30,53], S.K. Mandal[78], A. Manea[63], V. Manko[139], A.K. Manna[48], F. Manso[125], G. Mantzaridis[94], V. Manzari[50], Y. Mao[6], R.W. Marcjan[2], G.V. Margagliotti[23], A. Margotti[51], A. Marín[96], C. Markert[107], P. Martinengo[32], M.I. Martínez[44], G. Martínez García[102], M.P.P. Martins[32,109], S. Masciocchi[96], M. Masera[24], A. Masoni[52], L. Massacrier[129], O. Massen[59], A. Mastroserio[130,50], L. Mattei[24,125], S. Mattiazzo[27], A. Matyja[106], F. Mazzaschi[32], M. Mazzilli[31,114], Y. Melikyan[43], M. Melo[109], A. Menchaca-Rocha[67], J.E.M. Mendez[65], E. Meninno[101], M.W. Menzel[32,93], M. Meres[13], L. Micheletti[56], D. Mihai[112], D.L. Mihaylov[94], A.U. Mikalsen[20], K. Mikhaylov[140,139], L. Millot[72], N. Minafra[116], D. Miśkowiec[96], A. Modak[57,132], B. Mohanty[79], M. Mohisin Khan[VII,15], M.A. Molander[43], M.M. Mondal[79], S. Monira[134], D.A. Moreira De Godoy[124], A. Morsch[32], T. Mrnjavac[32], S. Mrozinski[64], V. Muccifora[49], S. Muhuri[133], A. Mulliri[22], M.G. Munhoz[109], R.H. Munzer[64], H. Murakami[122], L. Musa[32], J. Musinsky[60], J.W. Myrcha[134], B. Naik[121], A.I. Nambrath[18], B.K. Nandi[47], R. Nania[51], E. Nappi[50], A.F. Nassirpour[17], V. Nastase[112], A. Nath[93], N.F. Nathanson[82], C. Nattrass[120], K. Naumov[18], A. Neagu[19], L. Nellen[65], R. Nepeivoda[74], S. Nese[19], N. Nicassio[31], B.S. Nielsen[82], E.G. Nielsen[82], S. Nikolaev[139], V. Nikulin[139], F. Noferini[51], S. Noh[12], P. Nomokonov[140], J. Norman[117], N. Novitzky[86], J. Nystrand[20], M.R. Ockleton[117], M. Ogino[75], S. Oh[17], A. Ohlson[74], M. Oida[91], V.A. Okorokov[139], J. Oleniacz[134], C. Oppedisano[56], A. Ortiz Velasquez[65], H. Osanai[75], J. Otwinowski[106], M. Oya[91], K. Oyama[75], S. Padhan[47], D. Pagano[132,55], G. Paić[65], S. Paisano-Guzmán[44], A. Palasciano[50], I. Panasenko[74], P. Panigrahi[47], C. Pantouvakis[27], H. Park[123], J. Park[123], S. Park[103], T.Y. Park[138], J.E. Parkkila[134], P.B. Pati[82], Y. Patley[47], R.N. Patra[50], P. Paudel[116], B. Paul[133], H. Pei[6], T. Peitzmann[59], X. Peng[11], M. Pennisi[24], S. Perciballi[24], D. Peresunko[139], G.M. Perez[7], Y. Pestov[139], M. Petrovici[45], S. Piano[57], M. Pikna[13], P. Pillot[102], O. Pinazza[51,32], L. Pinsky[114], C. Pinto[32], S. Pisano[49], M. Płoskoń[73], M. Planinic[88], D.K. Plociennik[2], M.G. Poghosyan[86], B. Polichtchouk[139], S. Politano[32,24], N. Poljak[88], A. Pop[45],

JHEP12(2025)038

S. Porteboeuf-Houssais[125], I.Y. Pozos[44], K.K. Pradhan[48], S.K. Prasad[4], S. Prasad[48], R. Preghenella[51], F. Prino[56], C.A. Pruneau[135], I. Pshenichnov[139], M. Puccio[32], S. Pucillo[28,24], L. Quaglia[24], A.M.K. Radhakrishnan[48], S. Ragoni[14], A. Rai[136], A. Rakotozafindrabe[128], N. Ramasubramanian[126], L. Ramello[131,56], C.O. Ramírez-Álvarez[44], M. Rasa[26], S.S. Räsänen[43], R. Rath[96], M.P. Rauch[20], I. Ravasenga[32], K.F. Read[86,120], C. Reckziegel[111], A.R. Redelbach[38], K. Redlich[VIII,78], C.A. Reetz[96], H.D. Regules-Medel[44], A. Rehman[20], F. Reidt[32], H.A. Reme-Ness[37], K. Reygers[93], R. Ricci[28], M. Richter[20], A.A. Riedel[94], W. Riegler[32], A.G. Riffero[24], M. Rignanese[27], C. Ripoli[28], C. Ristea[63], M.V. Rodriguez[32], M. Rodríguez Cahuantzi[44], K. Røed[19], R. Rogalev[139], E. Rogochaya[140], D. Rohr[32], D. Röhrich[20], S. Rojas Torres[34], P.S. Rokita[134], G. Romanenko[25], F. Ronchetti[32], D. Rosales Herrera[44], E.D. Rosas[65], K. Roslon[134], A. Rossi[54], A. Roy[48], S. Roy[47], N. Rubini[51], J.A. Rudolph[83], D. Ruggiano[134], R. Rui[23], P.G. Russek[2], R. Russo[83], A. Rustamov[80], Y. Ryabov[139], A. Rybicki[106], L.C.V. Ryder[116], G. Ryu[71], J. Ryu[16], W. Rzesa[134], B. Sabiu[51], R. Sadek[73], S. Sadhu[42], S. Sadovsky[139], S. Saha[79], B. Sahoo[48], R. Sahoo[48], D. Sahu[65], P.K. Sahu[61], J. Saini[133], K. Sajdakova[36], S. Sakai[123], S. Sambyal[90], D. Samitz[101], I. Sanna[32,94], T.B. Saramela[109], D. Sarkar[82], P. Sarma[41], V. Sarritzu[22], V.M. Sarti[94], M.H.P. Sas[32], S. Sawan[79], E. Scapparone[51], J. Schambach[86], H.S. Scheid[32], C. Schiaua[45], R. Schicker[93], F. Schlepper[32,93], A. Schmah[96], C. Schmidt[96], M. Schmidt[92], N.V. Schmidt[86], A.R. Schmier[120], J. Schoengarth[64], R. Schotter[101], A. Schröter[38], J. Schukraft[32], K. Schweda[96], G. Scioli[25], E. Scomparin[56], J.E. Seger[14], Y. Sekiguchi[122], D. Sekihata[122], M. Selina[83], I. Selyuzhenkov[96], S. Senyukov[127], J.J. Seo[93], D. Serebryakov[139], L. Serkin[IX,65], L. Šerkšnytė[94], A. Sevcenco[63], T.J. Shaba[68], A. Shabetai[102], R. Shahoyan[32], B. Sharma[90], D. Sharma[47], H. Sharma[54], M. Sharma[90], S. Sharma[90], T. Sharma[41], U. Sharma[90], A. Shatat[129], O. Sheibani[135], K. Shigaki[91], M. Shimomura[76], S. Shirinkin[139], Q. Shou[39], Y. Sibiriak[139], S. Siddhanta[52], T. Siemiarczuk[78], T.F. Silva[109], W.D. Silva[109], D. Silvermyr[74], T. Simantathammakul[104], R. Simeonov[35], B. Singh[90], B. Singh[94], K. Singh[48], R. Singh[79], R. Singh[54,96], S. Singh[15], V.K. Singh[133], V. Singhal[133], T. Sinha[98], B. Sitar[13], M. Sitta[131,56], T.B. Skaali[19], G. Skorodumovs[93], N. Smirnov[136], R.J.M. Snellings[59], E.H. Solheim[19], C. Sonnabend[32,96], J.M. Sonneveld[83], F. Soramel[27], A.B. Soto-Hernandez[87], R. Spijkers[83], I. Sputowska[106], J. Staa[74], J. Stachel[93], I. Stan[63], T. Stellhorn[124], S.F. Stiefelmaier[93], D. Stocco[102], I. Storehaug[19], N.J. Strangmann[64], P. Stratmann[124], S. Strazzi[25], A. Sturniolo[30,53], A.A.P. Suaide[109], C. Suire[129], A. Suiu[32,112], M. Sukhanov[140], M. Suljic[32], R. Sultanov[139], V. Sumberia[90], S. Sumowidagdo[81], N.B.Sundstrom[59], L.H. Tabares[7], S.F. Taghavi[94], J. Takahashi[110], G.J. Tambave[79], Z. Tang[118], J. Tanwar[89], J.D. Tapia Takaki[116], N. Tapus[112], L.A. Tarasovicova[36], M.G. Tarzila[45], A. Tauro[32], A. Tavira García[129], G. Tejeda Muñoz[44], L. Terlizzi[24], C. Terrevoli[50], D. Thakur[24], S. Thakur[4], M. Thogersen[19], D. Thomas[107], N. Tiltmann[32,124], A.R. Timmins[114], A. Toia[64], R. Tokumoto[91], S. Tomassini[25], K. Tomohiro[91], N. Topilskaya[139], M. Toppi[49], V.V. Torres[102], A. Trifiró[30,53], T. Triloki[95], A.S. Triolo[32,53], S. Tripathy[32], T. Tripathy[125], S. Trogolo[24], V. Trubnikov[3], W.H. Trzaska[115], T.P. Trzcinski[134], C. Tsolanta[19], R. Tu[39], A. Tumkin[139], R. Turrisi[54], T.S. Tveter[19], K. Ullaland[20], B. Ulukutlu[94], S. Upadhyaya[106], A. Uras[126], M. Urioni[23],

JHEP12(2025)038

G.L. Usai[22], M. Vaid[90], M. Vala[36], N. Valle[55], L.V.R. van Doremalen[59], M. van Leeuwen[83], C.A. van Veen[93], R.J.G. van Weelden[83], D. Varga[46], Z. Varga[136], P. Vargas Torres[65], M. Vasileiou[77], A. Vasiliev[I,139], O. Vázquez Doce[49], O. Vazquez Rueda[114], V. Vechernin[139], P. Veen[128], E. Vercellin[24], R. Verma[47], R. Vértesi[46], M. Verweij[59], L. Vickovic[33], Z. Vilakazi[121], O. Villalobos Baillie[99], A. Villani[23], A. Vinogradov[139], T. Virgili[28], M.M.O. Virta[115], A. Vodopyanov[140], M.A. Völkl[99], S.A. Voloshin[135], G. Volpe[31], B. von Haller[32], I. Vorobyev[32], N. Vozniuk[140], J. Vrláková[36], J. Wan[39], C. Wang[39], D. Wang[39], Y. Wang[39], Y. Wang[6], Z. Wang[39], A. Wegrzynek[32], F. Weiglhofer[32,38], S.C. Wenzel[32], J.P. Wessels[124], P.K. Wiacek[2], J. Wiechula[64], J. Wikne[19], G. Wilk[78], J. Wilkinson[96], G.A. Willems[124], B. Windelband[93], J. Witte[93], M. Wojnar[2], J.R. Wright[107], C.-T. Wu[6,27], W. Wu[39], Y. Wu[118], K. Xiong[39], Z. Xiong[118], L. Xu[126,6], R. Xu[6], A. Yadav[42], A.K. Yadav[133], Y. Yamaguchi[91], S. Yang[58], S. Yang[20], S. Yano[91], E.R. Yeats[18], J. Yi[6], R. Yin[39], Z. Yin[6], I.-K. Yoo[16], J.H. Yoon[58], H. Yu[12], S. Yuan[20], A. Yuncu[93], V. Zaccolo[23], C. Zampolli[32], F. Zanone[93], N. Zardoshti[32], P. Závada[62], B. Zhang[93], C. Zhang[128], L. Zhang[39], M. Zhang[125,6], M. Zhang[27,6], S. Zhang[39], X. Zhang[6], Y. Zhang[118], Y. Zhang[118], Z. Zhang[6], M. Zhao[10], V. Zherebchevskii[139], Y. Zhi[10], D. Zhou[6], Y. Zhou[82], J. Zhu[39], S. Zhu[96,118], Y. Zhu[6], A. Zingaretti[54], S.C. Zugravel[56], N. Zurlo[132,55]

[1] *A.I. Alikhanyan National Science Laboratory (Yerevan Physics Institute) Foundation, Yerevan, Armenia*
[2] *AGH University of Krakow, Cracow, Poland*
[3] *Bogolyubov Institute for Theoretical Physics, National Academy of Sciences of Ukraine, Kyiv, Ukraine*
[4] *Bose Institute, Department of Physics and Centre for Astroparticle Physics and Space Science (CAPSS), Kolkata, India*
[5] *California Polytechnic State University, San Luis Obispo, California, U.S.A.*
[6] *Central China Normal University, Wuhan, China*
[7] *Centro de Aplicaciones Tecnológicas y Desarrollo Nuclear (CEADEN), Havana, Cuba*
[8] *Centro de Investigación y de Estudios Avanzados (CINVESTAV), Mexico City and Mérida, Mexico*
[9] *Chicago State University, Chicago, Illinois, U.S.A.*
[10] *China Nuclear Data Center, China Institute of Atomic Energy, Beijing, China*
[11] *China University of Geosciences, Wuhan, China*
[12] *Chungbuk National University, Cheongju, South Korea*
[13] *Comenius University Bratislava, Faculty of Mathematics, Physics and Informatics, Bratislava, Slovak Republic*
[14] *Creighton University, Omaha, Nebraska, U.S.A.*
[15] *Department of Physics, Aligarh Muslim University, Aligarh, India*
[16] *Department of Physics, Pusan National University, Pusan, South Korea*
[17] *Department of Physics, Sejong University, Seoul, South Korea*
[18] *Department of Physics, University of California, Berkeley, California, U.S.A.*
[19] *Department of Physics, University of Oslo, Oslo, Norway*
[20] *Department of Physics and Technology, University of Bergen, Bergen, Norway*
[21] *Dipartimento di Fisica, Università di Pavia, Pavia, Italy*
[22] *Dipartimento di Fisica dell'Università and Sezione INFN, Cagliari, Italy*
[23] *Dipartimento di Fisica dell'Università and Sezione INFN, Trieste, Italy*
[24] *Dipartimento di Fisica dell'Università and Sezione INFN, Turin, Italy*
[25] *Dipartimento di Fisica e Astronomia dell'Università and Sezione INFN, Bologna, Italy*
[26] *Dipartimento di Fisica e Astronomia dell'Università and Sezione INFN, Catania, Italy*
[27] *Dipartimento di Fisica e Astronomia dell'Università and Sezione INFN, Padova, Italy*
[28] *Dipartimento di Fisica 'E.R. Caianiello' dell'Università and Gruppo Collegato INFN, Salerno, Italy*
[29] *Dipartimento DISAT del Politecnico and Sezione INFN, Turin, Italy*

JHEP12(2025)038

[30] *Dipartimento di Scienze MIFT, Università di Messina, Messina, Italy*
[31] *Dipartimento Interateneo di Fisica 'M. Merlin' and Sezione INFN, Bari, Italy*
[32] *European Organization for Nuclear Research (CERN), Geneva, Switzerland*
[33] *Faculty of Electrical Engineering, Mechanical Engineering and Naval Architecture, University of Split, Split, Croatia*
[34] *Faculty of Nuclear Sciences and Physical Engineering, Czech Technical University in Prague, Prague, Czech Republic*
[35] *Faculty of Physics, Sofia University, Sofia, Bulgaria*
[36] *Faculty of Science, P.J. Šafárik University, Košice, Slovak Republic*
[37] *Faculty of Technology, Environmental and Social Sciences, Bergen, Norway*
[38] *Frankfurt Institute for Advanced Studies, Johann Wolfgang Goethe-Universität Frankfurt, Frankfurt, Germany*
[39] *Fudan University, Shanghai, China*
[40] *Gangneung-Wonju National University, Gangneung, South Korea*
[41] *Gauhati University, Department of Physics, Guwahati, India*
[42] *Helmholtz-Institut für Strahlen- und Kernphysik, Rheinische Friedrich-Wilhelms-Universität Bonn, Bonn, Germany*
[43] *Helsinki Institute of Physics (HIP), Helsinki, Finland*
[44] *High Energy Physics Group, Universidad Autónoma de Puebla, Puebla, Mexico*
[45] *Horia Hulubei National Institute of Physics and Nuclear Engineering, Bucharest, Romania*
[46] *HUN-REN Wigner Research Centre for Physics, Budapest, Hungary*
[47] *Indian Institute of Technology Bombay (IIT), Mumbai, India*
[48] *Indian Institute of Technology Indore, Indore, India*
[49] *INFN, Laboratori Nazionali di Frascati, Frascati, Italy*
[50] *INFN, Sezione di Bari, Bari, Italy*
[51] *INFN, Sezione di Bologna, Bologna, Italy*
[52] *INFN, Sezione di Cagliari, Cagliari, Italy*
[53] *INFN, Sezione di Catania, Catania, Italy*
[54] *INFN, Sezione di Padova, Padova, Italy*
[55] *INFN, Sezione di Pavia, Pavia, Italy*
[56] *INFN, Sezione di Torino, Turin, Italy*
[57] *INFN, Sezione di Trieste, Trieste, Italy*
[58] *Inha University, Incheon, South Korea*
[59] *Institute for Gravitational and Subatomic Physics (GRASP), Utrecht University/Nikhef, Utrecht, Netherlands*
[60] *Institute of Experimental Physics, Slovak Academy of Sciences, Košice, Slovak Republic*
[61] *Institute of Physics, Homi Bhabha National Institute, Bhubaneswar, India*
[62] *Institute of Physics of the Czech Academy of Sciences, Prague, Czech Republic*
[63] *Institute of Space Science (ISS), Bucharest, Romania*
[64] *Institut für Kernphysik, Johann Wolfgang Goethe-Universität Frankfurt, Frankfurt, Germany*
[65] *Instituto de Ciencias Nucleares, Universidad Nacional Autónoma de México, Mexico City, Mexico*
[66] *Instituto de Física, Universidade Federal do Rio Grande do Sul (UFRGS), Porto Alegre, Brazil*
[67] *Instituto de Física, Universidad Nacional Autónoma de México, Mexico City, Mexico*
[68] *iThemba LABS, National Research Foundation, Somerset West, South Africa*
[69] *Jeonbuk National University, Jeonju, South Korea*
[70] *Johann-Wolfgang-Goethe Universität Frankfurt Institut für Informatik, Fachbereich Informatik und Mathematik, Frankfurt, Germany*
[71] *Korea Institute of Science and Technology Information, Daejeon, South Korea*
[72] *Laboratoire de Physique Subatomique et de Cosmologie, Université Grenoble-Alpes, CNRS-IN2P3, Grenoble, France*
[73] *Lawrence Berkeley National Laboratory, Berkeley, California, U.S.A.*
[74] *Lund University Department of Physics, Division of Particle Physics, Lund, Sweden*
[75] *Nagasaki Institute of Applied Science, Nagasaki, Japan*

JHEP12(2025)038

[76] Nara Women's University (NWU), Nara, Japan
[77] National and Kapodistrian University of Athens, School of Science, Department of Physics, Athens, Greece
[78] National Centre for Nuclear Research, Warsaw, Poland
[79] National Institute of Science Education and Research, Homi Bhabha National Institute, Jatni, India
[80] National Nuclear Research Center, Baku, Azerbaijan
[81] National Research and Innovation Agency — BRIN, Jakarta, Indonesia
[82] Niels Bohr Institute, University of Copenhagen, Copenhagen, Denmark
[83] Nikhef, National institute for subatomic physics, Amsterdam, Netherlands
[84] Nuclear Physics Group, STFC Daresbury Laboratory, Daresbury, U.K.
[85] Nuclear Physics Institute of the Czech Academy of Sciences, Husinec-Řež, Czech Republic
[86] Oak Ridge National Laboratory, Oak Ridge, Tennessee, U.S.A.
[87] Ohio State University, Columbus, Ohio, U.S.A.
[88] Physics department, Faculty of science, University of Zagreb, Zagreb, Croatia
[89] Physics Department, Panjab University, Chandigarh, India
[90] Physics Department, University of Jammu, Jammu, India
[91] Physics Program and International Institute for Sustainability with Knotted Chiral Meta Matter (WPI-SKCM^2), Hiroshima University, Hiroshima, Japan
[92] Physikalisches Institut, Eberhard-Karls-Universität Tübingen, Tübingen, Germany
[93] Physikalisches Institut, Ruprecht-Karls-Universität Heidelberg, Heidelberg, Germany
[94] Physik Department, Technische Universität München, Munich, Germany
[95] Politecnico di Bari and Sezione INFN, Bari, Italy
[96] Research Division and ExtreMe Matter Institute EMMI, GSI Helmholtzzentrum für Schwerionenforschung GmbH, Darmstadt, Germany
[97] Saga University, Saga, Japan
[98] Saha Institute of Nuclear Physics, Homi Bhabha National Institute, Kolkata, India
[99] School of Physics and Astronomy, University of Birmingham, Birmingham, U.K.
[100] Sección Física, Departamento de Ciencias, Pontificia Universidad Católica del Perú, Lima, Peru
[101] Stefan Meyer Institut für Subatomare Physik (SMI), Vienna, Austria
[102] SUBATECH, IMT Atlantique, Nantes Université, CNRS-IN2P3, Nantes, France
[103] Sungkyunkwan University, Suwon City, South Korea
[104] Suranaree University of Technology, Nakhon Ratchasima, Thailand
[105] Technical University of Košice, Košice, Slovak Republic
[106] The Henryk Niewodniczanski Institute of Nuclear Physics, Polish Academy of Sciences, Cracow, Poland
[107] The University of Texas at Austin, Austin, Texas, U.S.A.
[108] Universidad Autónoma de Sinaloa, Culiacán, Mexico
[109] Universidade de São Paulo (USP), São Paulo, Brazil
[110] Universidade Estadual de Campinas (UNICAMP), Campinas, Brazil
[111] Universidade Federal do ABC, Santo Andre, Brazil
[112] Universitatea Nationala de Stiinta si Tehnologie Politehnica Bucuresti, Bucharest, Romania
[113] University of Derby, Derby, U.K.
[114] University of Houston, Houston, Texas, U.S.A.
[115] University of Jyväskylä, Jyväskylä, Finland
[116] University of Kansas, Lawrence, Kansas, U.S.A.
[117] University of Liverpool, Liverpool, U.K.
[118] University of Science and Technology of China, Hefei, China
[119] University of South-Eastern Norway, Kongsberg, Norway
[120] University of Tennessee, Knoxville, Tennessee, U.S.A.
[121] University of the Witwatersrand, Johannesburg, South Africa
[122] University of Tokyo, Tokyo, Japan
[123] University of Tsukuba, Tsukuba, Japan
[124] Universität Münster, Institut für Kernphysik, Münster, Germany
[125] Université Clermont Auvergne, CNRS/IN2P3, LPC, Clermont-Ferrand, France
[126] Université de Lyon, CNRS/IN2P3, Institut de Physique des 2 Infinis de Lyon, Lyon, France

JHEP12(2025)038

[127] Université de Strasbourg, CNRS, IPHC UMR 7178, F-67000 Strasbourg, France, Strasbourg, France
[128] Université Paris-Saclay, Centre d'Etudes de Saclay (CEA), IRFU, Départment de Physique Nucléaire (DPhN), Saclay, France
[129] Université Paris-Saclay, CNRS/IN2P3, IJCLab, Orsay, France
[130] Università degli Studi di Foggia, Foggia, Italy
[131] Università del Piemonte Orientale, Vercelli, Italy
[132] Università di Brescia, Brescia, Italy
[133] Variable Energy Cyclotron Centre, Homi Bhabha National Institute, Kolkata, India
[134] Warsaw University of Technology, Warsaw, Poland
[135] Wayne State University, Detroit, Michigan, U.S.A.
[136] Yale University, New Haven, Connecticut, U.S.A.
[137] Yildiz Technical University, Istanbul, Turkey
[138] Yonsei University, Seoul, South Korea
[139] Affiliated with an institute formerly covered by a cooperation agreement with CERN
[140] Affiliated with an international laboratory covered by a cooperation agreement with CERN.

[I] Deceased
[II] Also at: Max-Planck-Institut fur Physik, Munich, Germany
[III] Also at: Czech Technical University in Prague (CZ)
[IV] Also at: Italian National Agency for New Technologies, Energy and Sustainable Economic Development (ENEA), Bologna, Italy
[V] Also at: Instituto de Fisica da Universidade de Sao Paulo
[VI] Also at: Dipartimento DET del Politecnico di Torino, Turin, Italy
[VII] Also at: Department of Applied Physics, Aligarh Muslim University, Aligarh, India
[VIII] Also at: Institute of Theoretical Physics, University of Wroclaw, Poland
[IX] Also at: Facultad de Ciencias, Universidad Nacional Autónoma de México, Mexico City, Mexico

JHEP12(2025)038